2020

# SYNTHESIS AND BIOCHEMICAL EVALUATION OF HETEROARYL CJOC42 DERIVATIVES FOR GANKYRIN BINDING

Yi-Chih Juang

# SYNTHESIS AND BIOCHEMICAL EVALUATION OF HETEROARYL CJOC42 DERIVATIVES FOR GANKYRIN BINDING

A theses submitted in partial fulfillment
of the requirement for the degree of

MASTER OF SCIENCE

to the faculty of the

DEPARTMENT OF CHEMISTRY

of

ST. JOHN'S COLLEGE OF LIBEREAL ARTS AND SCIENCES

at

ST. JOHN'S UNIVERSITY
New York

by

Daniel (Yi-Chih) Juang

Submitted Date: July 22nd 2020

Approved Date: September 1st 2020

Daniel (Yi-Chih) Juang

Dr. Aaron Muth

**ABSTRACT**

SYNTHESIS AND BIOCHEMICAL EVALUATION OF HETEROARYL CJOC42 DERIVATIVES FOR GANKYRIN BINDING

Daniel (Yi-Chih) Juang

Gankyrin is an oncogenic protein directly involved in various biological processes, such as cellular growth, cell cycle progression, cell proliferation, and invasion. Gankyrin overexpression has been observed in many cancer types, and gankyrin either directly or indirectly regulates key biochemical pathways related to cancer progression through its various protein-protein interactions (PPIs). Gankyrin interacts with retinoblastoma protein (pRb), cyclin-dependent kinase 4 (CDK4), mouse double minute2 (MDM2) and the S6 ATPase of the 19S regulatory cap of the 26S proteasome. Each of these PPIs controls the degradation of key tumour suppressor proteins, which in turn controls cell proliferation, migration and metastasis. Overexpression of gankyrin in cancer cells is directly linked to these cellular activities. The first non-peptide-based small inhibitor, cjoc42, was discovered in 2016 and inhibited the binding of gankyrin and the S6 ATPase of the 26S proteasome leading to diminished proliferation in certain cancers. Despite this advance, cjoc42 has 2 major flaws: low binding affinity and poor water solubility. In order to improve on the cjoc42 scaffold and address these issues, a series of heterocycles were introduced to the cjoc42 scaffold. Herein we describe the synthesis and biological evaluation of these next-generation cjoc42-based gankyrin inhibitors.

**ACKNOWLEDGEMENTS**

I am extremely delighted to acknowledge the utmost support and assistance of my mentor, Dr. Aaron Muth for his guidance throughout my research. With his vast knowledge Dr. Aaron Muth always inspired, encouraged and supervised my work, and I would like to offer my sincerest gratitude towards him. I would like to offer special thanks to Dr. Philip Lukeman and Dr. David Brown for being members of my defence committee and providing their valuable time. I would like to thank each of my family member especially to my loyal and lovely dog Sunny for their endless love and blessings. I would like to extend my gratefulness to all of my lab mates who have been tremendously helpful in and out of the laboratory. I am also thankful to my colleagues for their support. I am thankful to both Chemistry and Pharmacy department for supporting me throughout my studies. Lastly, I would like to thank god without whom none of this would be possible.

## TABLE OF CONTENTS

## LIST OF TABLES

## LIST OF FIGURES

## LIST OF SCHEMES

## 1. Introduction

### 1.1: Protein-protein interactions (PPIs)

Protein-protein interactions (PPIs) are crucial in cells and living organisms to their proper functioning. It occurs when protein molecules physically interact with each other at specific binding regions. These interactions play important roles in many cellular functions, such as: cell cycle control, cell to cell interaction, metabolic processes, and cellular development.[1] At a molecular level, PPIs regulate cell-to-cell communication, receptor-ligand interactions, signal transduction pathways, gene transcription, and proliferation.[2] Aberrant behaviour of these PPIs has been linked to the onset and development of numerous types of cancers as well as other diseases, where cancer is when cells uncontrollably divide, proliferate, and spread to other regions of the body.[3] Therefore, PPIs have become a target for anticancer therapeutic strategies due to our fuller understanding of their cancer biology.[4]

Challenges and concerns have long been known when targeting PPIs despite being an attractive anticancer strategy. Some of these challenges include: large PPI interface areas, lack of a deep binding region, close or adjacent binding regions, and a lack of natural ligands as PPI inhibitors.[4] Despite these challenges, great advances have been made in this area with some PPI-targeting compounds currently in clinical trials. For example, ABT-737 (**Figure 1**.) is a small molecule inhibitor of the Bcl-2/BAK interaction, which has shown to be cytotoxic to multiple myeloma cell lines.[5] ABT-263 (**Figure 1**.) and ABT-199 (**Figure 1**.) are also small molecule inhibitors currently in clinical trials which target Bcl-2-BAK interaction/ in certain tumors.[6,7] 17-AAG (**Figure 1**.) is a potent inhibitor of the heat shock protein 90/HIF1α interaction, which is used for the treatment of HER-2 positive

metastatic breast cancers.[8] The nutlin family of compounds are small molecule inhibitors of the mouse double minute 2 homolog (MDM2)/p53 interaction for the treatment of multiple myeloma.[9] These examples have demonstrated that small molecule inhibitors are in fact a very promising anticancer strategy going forward.

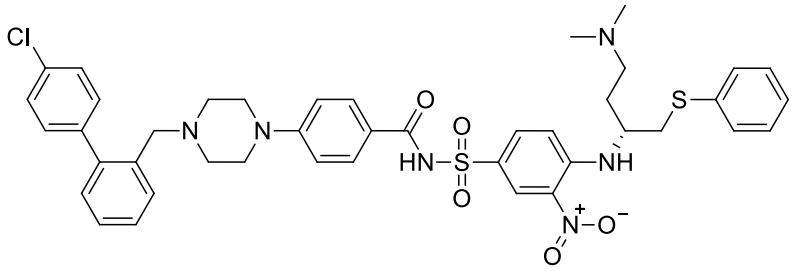

ABT-737

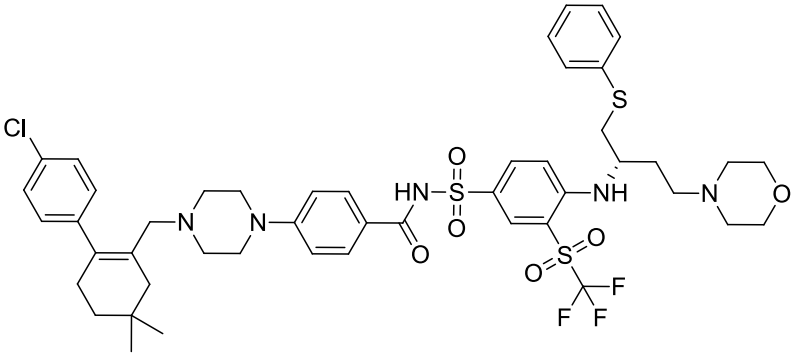

ABT-263

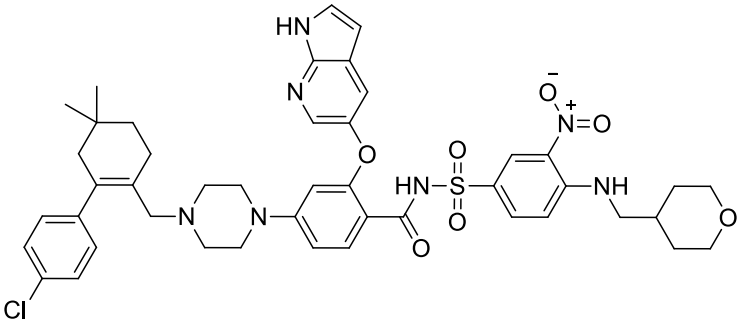

ABT-199

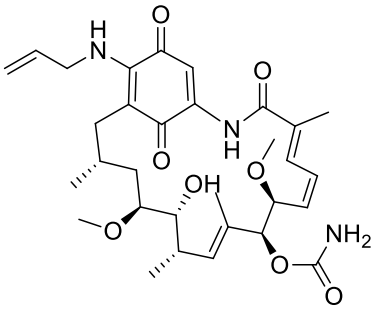

17-AAG

**Figure 1.** Structure of ABT-737, ABT-199, ABT-263, and 17-AAG.

### 1.2: Gankyrin

Gankyrin is an oncogenic protein that is involved in multiple PPIs which regulates various other cellular activities such as: cellular growth, cell cycle progression, proliferation, and invasion. Higashitsuji et al, identified the gene for gankyrin which is frequently overexpressed in cancerous hepatocytes.[10] Initially it was found that gankyrin binds to retinoblastoma protein (pRb), increasing its phosphorylation and subsequent degradation, resulting in increased cell growth which contributes to hepatocarcinogeneses.[11]

Gankyrin principally is a component of the 26 S proteasome and consists of 7 ankyrin repeats in its sequence while containing 226 amino acids resulting in a 25-kDa protein. Gankyrin is a regulatory subunit of the 26S proteasome which interacts with its S6 ATPase subunit. Gankyrin's function as a chaperone for the 26S proteasome is crucial in the proteasomal degradation of certain proteins.

Two key proteins which gankyrin directly interacts with are the tumour suppressor proteins retinoblastoma protein (pRb) and p53. Phosphorylation of pRb by cyclin-dependent kinase 4 (CDK4) is regulated by gankyrin, and ubiquitylation of p53 by MDM2 is enhanced by gankyrin.[12] pRb and p53 are both tumour suppressor proteins, and they function to inhibit cell proliferation and tumour development in normal cells. Recent studies have shown that overexpression of gankyrin is related to various cancer types. Specifically, overexpression of gankyrin is observed in cervical cancer[13], breast cancer[14], oesophageal squamous cell carcinoma (ESCC)[15], gastric cancer[16] as well as other cancer types. This finding in combination with evidence in the next section suggests demonstrates that gankyrin is important in numerous cancers. This demonstrates that gankyrin is

important to the progression of numerous human cancers and exhibits great promise as a therapeutic target for multiple cancer types.

### 1.2.1: The gankyrin-proteasome interaction

The 26S proteasome is a large ATP-dependent protease complex involved in the degradation of ubiquitin-tagged proteins.[17] It consists of two sub-complexes, a 20S core particle and a 19S regulatory particle (**Figure 2**). It is responsible for many essential cellular processes which include: DNA replication, transcription, cell cycle maintenance, stress responses and signal transduction.[18] Gankyrin is a chaperone of the 26S proteasome ( **Figure 2**) and regulates various oncogenic signalling pathways in cancer cells by controlling the proteasomal degradation of numerous tumour suppressor proteins (e.g., pRb and p53). The 19S regulatory particle of the 26S proteasome consists of regulatory ATPase complexes which use the chemical energy from ATP hydrolysis to unfold proteins and shuttle them into the proteases' active site for degradation. The C-terminal portion of the S6 ATPase from the 26S proteasome is specifically responsible for interacting with gankyrin. Cells which overexpress gankyrin exhibit an increase in the degradation of pRb[19], p53 and other tumour suppressor proteins which ultimately leads to rapidly proliferating cells and cancer progression.

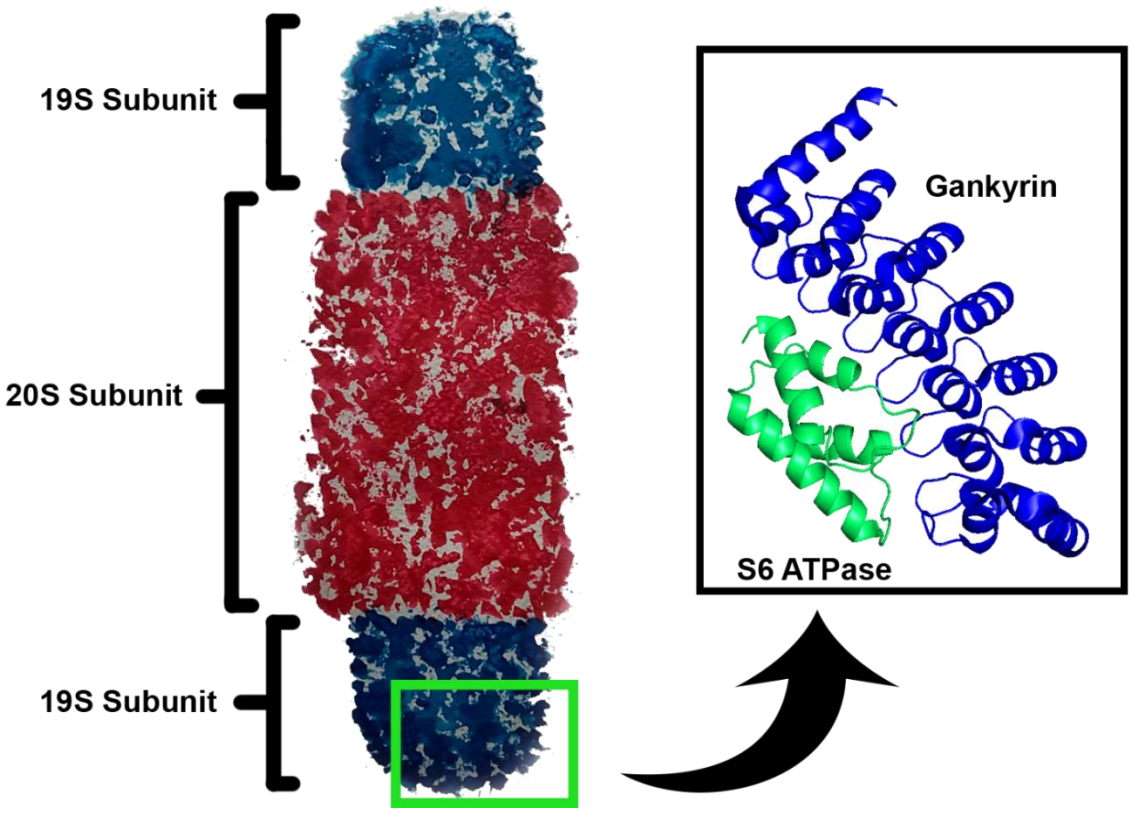


**Figure 2.** Structure and Subunits of the 26S Proteasome (Left). Gankyrin Binding of the S6 ATPase of the 26S Proteasome (Right).

### 1.2.2: Gankyrin's ability to bind and regulate pRb

pRb is a tumour suppressor protein which plays a role in controlling tumour progression as well as regulating the cell cycle.[20] Overexpressed gankyrin binds to CDK4 and pRb, resulting in increased phosphorylation and subsequent degradation of pRb.[19] pRb levels are typically regulated by CDK4 phosphorylation which inactivates the pRb's function.[21] However, gankyrin overexpression enhances phosphorylated pRb degradation as well as further promoting pRb phosphorylation by activating CDK4.[22] The relationship between pRb, CDK4, and gankyrin is shown in in **Figure 3a** and **3c**. Overactive CDKs are present in most cancer cells, and CDK both phosphorylates and inactivates pRb in normal and cancer cells.[23] . Gankyrin competes with p16 for binding CDK4, where p16 typically inhibits CDK4-mediated phosphorylation of pRb.[24] Therefore, overexpression of gankyrin negatively regulates pRb both directly and indirectly, which in turn enhances cell cycle progression and cell proliferation.

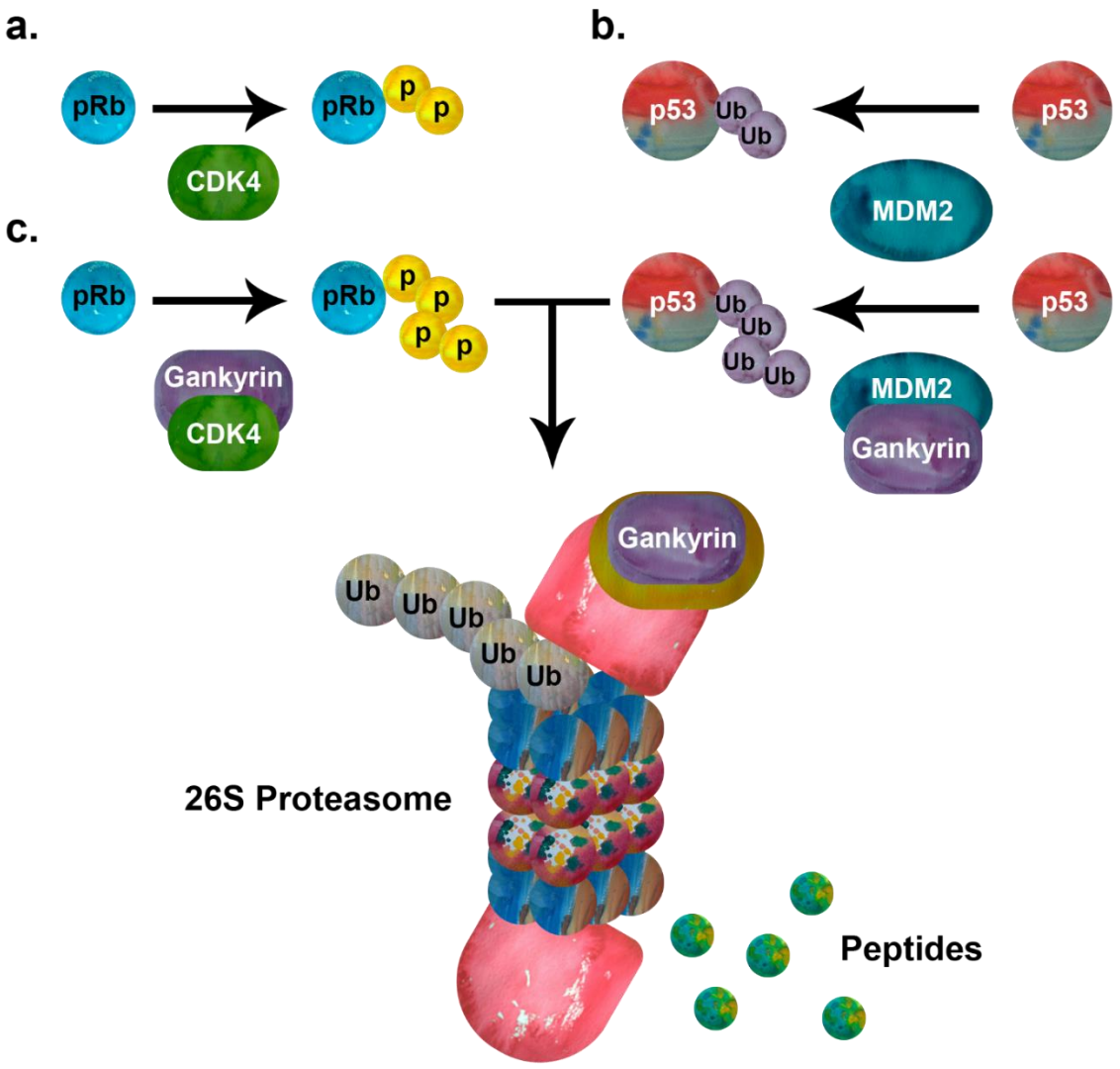


**Figure 3.** Gankyrin's Regulation of Tumour Suppressor Protein Degradation. (a) CDK4 Controls Phosphorylation of pRb. (b) MDM2 Regulates Ubiquitination of p53. (c) Elevated Gankyrin Levels Enhances Phosphorylation of pRb by Activating CDK4 and Enhances p53 Ubiquitination by Activating MDM2, leading to an increase of pRb and p53 Degradation by the 26S Proteasome.

### 1.2.3: Gankyrin-mediated degradation of p53

Gankyrin also regulates p53 levels by binding to and activating MDM2, which is a negative regulator of p53, a protein that regulates the cell cycle. (**Figure 3b**). p53 also controls a vast range of cellular processes by regulating ~500 target genes.[25] The gankyrin-MDM2 interaction ultimately facilitates p53-MDM2 binding, which increases the ubiquitylation and subsequent degradation of p53 by the 26S proteasome.[26, 27] Furthermore, ubiquitylated p53 is shuttled to the proteasome by gankyrin for subsequent degradation **(Figure 3c**). The indirect involvement of gankyrin in diminishing p53 levels ultimately results in uncontrolled cell growth, increased cell proliferation, negative regulation of apoptosis[28] and cancer progression in cancer cells.

### 1.2.4: Other gankyrin-based PPIs

Gankyrin is primarily involved in the degradation of pRb and p53, however, it also interacts with various other proteins. RelA, or transcription factor p65, can directly bind gankyrin, which in turn regulates the cellular inflammation which often precedes different cancers.[29] Gankyrin also binds to hepatocyte nuclear factor 4α (HNF4α), a nuclear transcription factor and tumour suppressor protein that is crucial for liver development and regulating liver cancer development. [30] Overexpressed gankyrin in hepatocellular carcinoma (HCC) cells competes for NRF2 binding with KEAP1, which inhibits proteasomal degradation of NRF2.[31] Disruption of the interaction between KEAP1 and gankyrin is a potential therapeutic target against HCC.[32] PPIs that involve gankyrin

regulate many cellular processes and pathways demonstrating the importance of research aimed at gaining a fuller understanding of gankyrin's biological role.

### 1.2.5: Overexpression of gankyrin in specific cancer types

Gankyrin is an important regulator of key cancer hallmarks such as: carcinogenesis, proliferation and metastasis. From its role in various cellular metabolic pathways, gankyrin overexpression also has a positive correlation with metastasis, proliferation and migration. Cell signalling pathways such as Wnt/β-Catenin, NF-κB, STAT3/Akt, IL-1β/IRAK-1 and RhoA/ROCK have all been found to be regulated by gankyrin.[33]

Gankyrin plays different roles in different types of cancers. In colorectal cancer, gankyrin regulates mTORC1 signalling and the PI3K/GSK-3β/β-catenin pathway, which promotes carcinogenesis and progression.[34] In gastric cancer, gankyrin activates the PI3K/AKT signalling pathway which promotes cancer cell proliferation.[35] Gankyrin also has an important role in cholangiocarcinoma by activating the IL-6/STAT3 signalling pathway through down-regulation of pRb.[36]

This active and prominent role in multiple cancer types shows gankyrin's important oncogenic roles, and therefore developing specific therapeutics for gankyrin overexpressing cancers could be a promising therapeutic strategy.

### 1.3: Gankyrin-binding molecules

There have been 3 primary methods utilized for developing gankyrin-targeting small molecules: synthesized protein-based inhibitors, peptide-based inhibitors and non-peptide-based small molecule inhibitors. The first gankyrin-binding molecule was identified as a synthetic derivative of the S6 ATPase of the 26S proteasome.[37] This molecule also demonstrated excellent binding affinity ($K_d$ = 21 nM) and was able to disrupt the gankyrin-26S proteasome interaction. However, protein based inhibitors are often too large in size to be developed as appropriate therapeutics and also possess poor membrane permeability as well as metabolic stability.[38] The first and only peptide-based inhibitor was developed in 2014. This peptide, amino acid sequence of EEVD (**Figure 4a**), was a key sequence of the S6 ATPase of the 26S proteasome for gankyrin binding, and this peptide inhibits the binding of the S6 ATPase with gankyrin. Despite this finding, EEVD was found to require high concentrations for effectively binding gankyrin, and peptide-based inhibitors typically are found to lack metabolic stability and cell permeability, suggesting that another approach was necessary for targeting gankyrin.

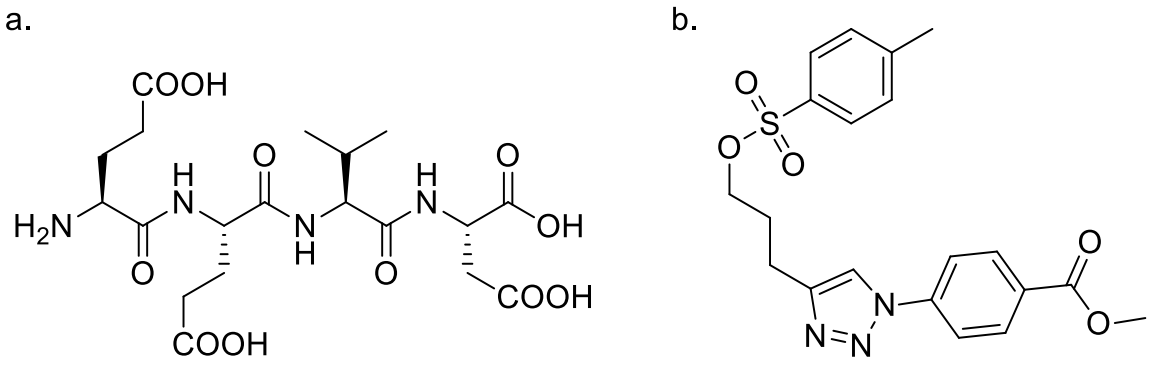


**Figure 4.** a.) Structure of the First Peptide-Based Gankyrin Binder EEVD. b.) Structure of the First Non-Peptide Based Small Molecule Binder of Gankyrin, cjoc42.

In 2016, cjoc42 **(Figure 4b**), the first non-peptide based small molecule binder of gankyrin, was discovered. It was discovered from a high throughput screen in 2016 and it was the very first small molecule binder of gankyrin ($K_d$ of 630 nM) which also prevents gankyrin binding with the 26S proteasome. The ability of cjoc42 to bind gankyrin was confirmed through the use of various experiments: thermal shift assay, microscale thermophoresis (MST) and isothermal calorimetry (ITC).[39] In addition, a chemical shift change from NMR studies of cjoc42 binding gankyrin suggested that cjoc42 binds to the specific site on gankyrin where it interacts with the 26S proteasome.[39] In U2OS and HepG2 cancer cell lines, cjoc42 was able to restore p53 levels, indicating disruption of the gankyrin-26S proteasome interaction.[39] This finding suggested that cjoc42 may show promise in inhibiting cancer cell proliferation in certain cancer types.[40] A follow up study showed that cjoc42 can indeed inhibit cancer cell proliferation in huh6 and hep1c1c7 hepatoblastoma cell lines.[40] In addition, this inhibition of proliferation was linked to increased p53, pRb and other tumour suppressor protein levels, against suggesting cjoc42 disrupts the gankyrin-26S proteasome interaction. With these findings, cjoc42 has demonstrated promise for targeting gankyrin and treating certain cancers. However, cjoc42 displays relatively weak gankyrin binding and poor water solubility. This provided an opportunity to continue to optimize the cjoc42 scaffold for gankyrin binding and water solubility.

The equilibrium dissociation constant ($K_d$) is a basic parameter utilized to evaluate the binding properties of a drug to a particular target.[41] The lower the $K_d$ value, the better the binding affinity., A typical $K_d$ value for a particular drug varies depending on the class of drugs and their respective targets. For example, a $K_d$ value of 1 mM could be considered

as high affinity in metabolic regulation, while it could be considered as low affinity in antibody design[42]. From the literature, the binding affinities of topoisomerase inhibitors have a range of $K_d$ values from 6-550 nM, depending on the particular drug class[43], therefore the goal of this project was to synthesise cjoc42 derivatives with lower $K_d$ values than cjoc42.

### 1.4: Hypothesis

1. Replacing the aryl triazole moiety of cjoc42 with heteroaryl triazole groups will improve water solubility while maintaining or improving gankyrin binding.
2. Replacing the tosyl group of cjoc42 with heteroaryl amides will improve water solubility while maintaining or improving gankyrin binding.

### 1.5: Design Rationale

As described earlier, cjoc42 has demonstrated promise as a gankyrin-binding therapeutic, but demonstrates poor gankyrin binding as well as poor water solubility. Therefore, these deficiencies became the focal points for this project. Cjoc42 (**Figure 4b**) contains a methyl benzoate group, triazole ring, *p*-tosylate group, and a propyl group linker. The methyl benzoate and *p*-tosylate were thought to be replaced with heteroaromatic ring systems to improve gankyrin binding while also improving water solubility. This enhanced binding could be achieved by improving hydrogen bonding with $R_{41}$ due to the presence of more polar aromatic heterocycles in these cjoc42 derivatives (**Figure 5**, Top). Factors

that could influence molecule binding includes electronic, steric or hydrogen bonding, therefore changing these factors could alter biochemical properties of cjoc42.

Previous work in our group was aimed at improving the metabolic stability of cjoc42, therefore a series of sulfonate ester replacements were synthesized and evaluated. From this, an amide group (**JA-1-33**, **Figure 5**) was found to be a suitable replacement by maintaining similar gankyrin binding to the sulfonate ester of cjoc42, while presumably also increasing metabolic stability. Both amides and sulphonate esters could potentially undergo hydrolysis by a similar mechanism, however the reaction with an amide is much slower[44].

The amide bond is considered a very non-reactive and stable functional group due to its ability to delocalize its electrons to the nitrogen, carbon, and oxygen atoms, which in turn makes the bond less polar and less susceptible to nucleophilic attack.[45] Sulphonate ester groups, however, are susceptible to nucleophilic attack[46], therefore replacing this functional group with the more stable amide could improve the overall stability of our next generation cjoc42 derivatives. The previously synthesized cjoc42 derivative **JA-1-33** (**Figure 5**) containing an amide replacement for the sulphonate ester displayed similar gankyrin binding affinity to cjoc42. Therefore, with similar gankyrin binding and potentially enhanced metabolic stability, the amide replacement was decided to be suitable for future derivatives. The binding affinity of cjoc42 derivatives were evaluated in a protein thermal shift assay. The solubility of cjoc42 derivatives were predicted by a clogP value, which were predicted by software calculations made by ChemDraw.

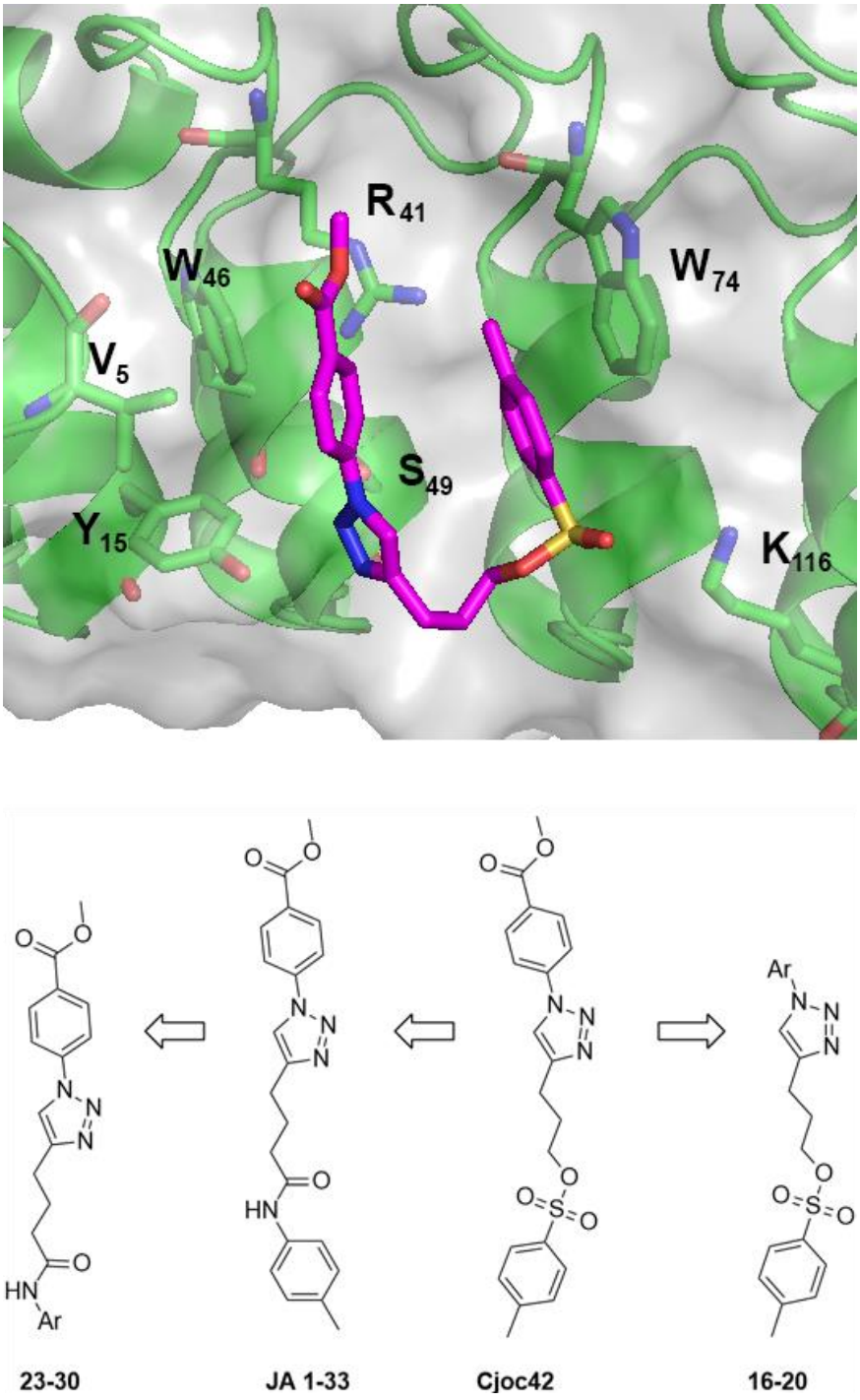


**Figure 5.** Top: Proposed binding of cjoc42 with gankyrin by molecular modelling. PDB: 2DVW. Bottom: Proposed Derivatives of cjoc42 (compounds **23-30** and **16-20**) for improved solubility and optimised Gankyrin Binding. Ar = Various Aromatic Heterocycles.

## 2. Experimental section

### 2.1: General chemistry

All reagents were directly used from commercial sources without further purification. Solvents used in all parts of chemistry and column chromatography were more than 99% pure and are also from commercial sources. A 400 MHz nuclear magnetic resonance spectrometer (NMR) were used for all proton ($^{1}H$) and carbon ($^{13}C$) spectra. A chemical shift of 2.5 ppm was used for residual DMSO-$d_6$ and a chemical shift of 7.26 ppm was used for residual $CDCl_3$ in all proton NMR spectra. Data are reported as follows: chemical shift (multiplicity [singlet (s), doublet (d), doublet of doublets (dd), doublet of doublets of doublets (ddd), triplet (t), quartet (q), quintet (p), sextet (h), multiplet (m)], coupling constants [Hz], integration). Carbon chemical shifts are reported in ppm with the respective solvent resonance as the internal standard (DMSO-$d_6$, 39.52 ppm or $CDCl_3$, 77.2 ppm). All NMR spectra were acquired at ambient temperature. Analytical thin-layer chromatography (TLC) was performed using Silica Gel 60 Å F254 precoated plates (0.25 mm thickness). Monitoring reactions by TLC or column chromatography were visualised by UV absorption with ether wavelength of 254 nm or 365 nm. HPLC was performed by normal phase column or reverse-phase C18 column with UV detector. Specifications for Ultra high performance LC.MS to collect mass spectrometry data are: reverse-phase C18 column (1.7 μm particle size, 2.1 x 50 mm), dual atmospheric pressure chemical ionization (API)/electrospray (ESI) mass spectrometry detector, and photodiode array detector.

### 2.2: HPLC Analysis

Agilent Eclipse plus C18 from Agilent 1260 infinity series HPLC system (Agilent, Santa Clara, CA) was used to analyse the purity of synthesised compounds, where 3.5 μm, 4.6 mm × 100 mm column were used and the runs were monitored at 254 nm. Target compounds were aimed to be at least 95% pure. The mobile phase consists of acetonitrile (ACN) and water (0.1% DEA). All gradient trials were run with various ratio of ACN and water for 10 minutes with the flow rate of 0.5 mL/minute for analysis of (**16**, **23**-**25**, **27**). For compounds (**17**-**20**, **26**, **28**-**30**) were analysed by UPLC. XBridge ® BEH shield RP 2.5 μm (3.0 x 100 mm) (Waters, MA, USA) column was used for UPLC analysis, where the runs were monitored at 254 nm for 5 minutes with flow rate of 0.5 ml/minute. Various ratios of acetonitrile (ACN) and water (0.1% FA) were used for the mobile phase.

### 2.3: LC/MS Analysis

Agilent Technologies 1260 infinity series LC were used for LR-LC/MS analysis, and all runs were performed on a single quadrupole. The following specifications were used on all runs for analysis: Column = Agilent Poroshell 120 EC-C18 2.7 μm, 4.6 x 50 mm.; temperature = 300 K; solvent acetonitrile/water 70:30 (0.1% formic acid): flow rate 0.5 mL/min; isocratic; 10 μL injection and 5 minutes for each run.

## 2.4: General Synthetic Methods

### 2.4.1: General synthetic procedure for azide intermediates (6-8)

To a stirred solution of 2-aminothiazole in HCl (6M, 1.2 eq) at 0˚C was added sodium nitrite (1.2 eq). The reaction mixture was stirred for 30 minutes at 0˚C, followed by addition of sodium azide (1.2 eq), and then the reaction mixture was stirred for an additional 15 minutes at room temperature. Upon completion, the reaction mixture was partitioned between the ethyl acetate and aqueous layers. The organic layer was then dried over sodium sulphate, filtered and removed under reduced pressure to obtain desired products **6-8** which were all immediately used in the next step without purification or further analysis.

### 2.4.2: 3-Azidopyridine (6)

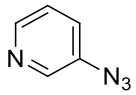


### 2.4.3: 2-Azidothiazole (7)

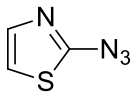


### 2.4.4: 5-Azido-2-methoxypyridine (8)

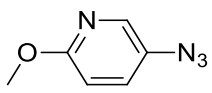

### 2.4.5: 4-Azidopyridine (9)

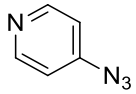

To a stirred solution of 4-bromopyridine (1 eq) in EtOH/$H_2O$ (1:1) was added NaOH (0.5 eq) and $NaN_3$ (2.3 eq), and the reaction mixture was stirred overnight at 100˚C. Upon completion, the reaction mixture was partitioned between the ethyl acetate and aqueous layers. The organic layer was then dried over sodium sulphate, filtered and removed under reduced pressure to obtain the desired product.[47] Yields were not obtained due to the instability of these compounds, therefore, the synthesised azide intermediates were used immediately for the next reaction.

### 2.4.6: 2-Azidopyridine (10)

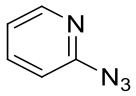

To a stirred solution of 2-chloropyridine (1 eq) in DMF was added $NH_4Cl$ (2 eq) and $NaN_3$ (2 eq), and the reaction mixture was stirred overnight in a pressure chamber at 110˚C. Upon completion, the reaction mixture was partitioned between ethyl acetate and the aqueous layer. The organic layer was then dried over sodium sulphate, filtered and removed under reduced pressure to obtain desired product.[48] Yields were not obtained due to the instability of these compounds, therefore, the synthesised azide intermediates were used immediately for the next reaction.

### 2.4.7: General synthetic procedure for intermediates (11-15)

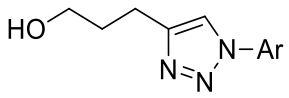


Ar = various aromatic heterocycles

Azides **6-10** (1 eq) were each dissolved in a THF/t-BuOH/ water (2:3:5) mixture, to which 4-pentyn-1-ol (1 eq), copper sulphate (0.3 M, 0.3 eq), and sodium ascorbate (0.1 M, 0.01 eq) were added. The reaction mixture was then stirred overnight at room temperature. Upon completion, the reaction mixture was partitioned between ethyl acetate and water, and then washed 3 times with water. The organic layer was then dried over sodium sulphate, filtered and concentrated under reduced pressure to obtain desired alcohol intermediate (**11-15**) in varying yields (3-42%).

### 2.4.8: 3-(4-(3-hydroxypropyl)-1*H*-1,2,3-triazol-1-yl)pyridine (11)

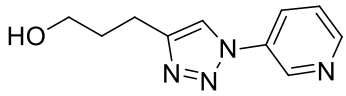


(371mg, 22%). $^{1}$H NMR (400 MHz, DMSO-$d_6$) δ= 9.12 (d, *J* = 2.5 Hz, 1H), 8.67 (d, 2H), 8.30 (ddd, *J* = 8.3, 2.5, 1.4 Hz, 1H), 7.64 (dd, *J* = 8.3, 4.8 Hz, 1H), 4.55 (s, 1H), 3.49 (t, *J* = 6.3 Hz, 2H), 2.76 (t, 2H), 1.87 – 1.77 (m, 2H). $^{13}$C NMR (100 MHz, DMSO-$d_6$) δ= 149.34, 148.39, 141.02, 133.43, 127.53, 124.54, 120.42, 60.02, 32.07, 21.68.

**2.4.9: 4-(4-(3-hydroxypropyl)-1*H*-1,2,3-triazol-1-yl)pyridine (12)**

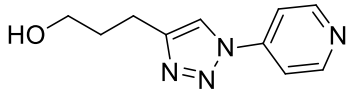

(314mg, 42%). $^{1}$H NMR (400 MHz, DMSO-$d_6$) δ= 8.80 – 8.74 (m, 3H), 7.95 (d, *J* = 6.3 Hz, 2H), 4.55 (t, *J* = 5.0 Hz, 1H), 3.48 (m, 2H), 2.76 (t, *J* = 7.7 Hz, 2H), 1.87 – 1.78 (m, 2H). $^{13}$C NMR (100 MHz, DMSO-$d_6$) δ= 149.14, 148.95, 144.79, 120.49, 114.25, 59.89, 31.84, 21.59.

**2.4.10: 2-(4-(3-hydroxypropyl)-1*H*-1,2,3-triazol-1-yl)thiazole (13)**

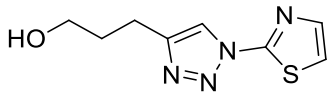

(76mg, 3%). $^{1}$H NMR (400 MHz, DMSO-$d_6$) δ= 8.64 (s, 1H), 7.81 (d, *J* = 3.4 Hz, 1H), 7.74 (d, *J* = 3.4 Hz, 1H), 4.55 (t, *J* = 5.1 Hz, 0H), 3.46 (q, *J* = 11.7, 6.0 Hz, 2H), 2.76 (t, *J* = 7.7 Hz, 2H), 1.86 – 1.76 (m, 2H). $^{13}$C NMR (101 MHz, DMSO-$d_6$) δ 156.92, 148.64, 140.53, 119.65, 119.45, 59.86, 31.85, 21.48.

### 2.4.11: 2-(4-(3-hydroxypropyl)-1*H*-1,2,3-triazol-1-yl)pyridine (14)

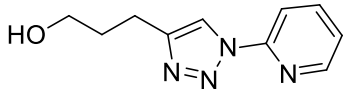


(177mg, 10%). $^{1}$H NMR (400 MHz, DMSO-$d_6$) δ 8.62 – 8.56 (m, 2H), 8.12 – 8.07 (m, 2H), 7.53 (s, 1H), 4.55 (t, *J* = 5.1 Hz, 1H), 3.47 (q, *J* = 11.4, 6.2 Hz, 2H), 2.76 (t, *J* = 7.7 Hz, 2H), 1.86 – 1.77 (m, 2H). $^{13}$C NMR (101 MHz, DMSO-$d_6$) δ 148.81, 148.67, 148.05, 139.95, 123.93, 118.87, 113.44, 59.98, 32.03, 21.61.

### 2.4.12: General synthetic procedure for sulfonate esters (16-20)

To a stirred solution of the desired alcohol intermediate (**11-15**, 1 eq) in dichloromethane (10 mL) at 0˚C was added triethylamine (1 eq) and 4-dimethylaminopyridine (0.1 eq). *p*-tosyl chloride (1.5 eq) was then added and the reaction mixture was stirred for an additional 15 minutes at 0˚C, followed by stirring overnight at room temperature. Upon completion, the reaction mixture was partitioned between dichloromethane and water. The organic layer was then washed 3 times with water, dried over sodium sulfate, filtered, and removed under reduced pressure. The desired sulphonate esters **(16-20)** were then purified using column chromatography and obtained in modest to good yields (19%-57%).

**2.4.13: 2-(4-(3-(tosyloxy) propyl)-1H-1,2,3-triazol-1-yl)methoxypyridine (16)**

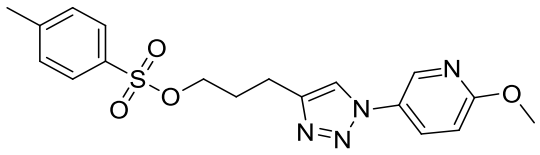

(22 mg, 13%). $^{1}$H NMR (400 MHz, $CDCl_3$) δ= 8.41 (d, *J* = 2.8 Hz, 1H), 7.91 (dd, *J* = 8.9, 2.8 Hz, 1H), 7.76 (d, *J* = 8.0 Hz, 2H), 7.63 (s, 1H), 7.32 (d, *J* = 8.0 Hz, 2H), 6.87 (d, *J* = 8.9 Hz, 1H), 4.07 (t, *J* = 6.0 Hz, 2H), 3.98 (s, 3H), 2.86 (t, *J* = 7.3 Hz, 2H), 2.41 (s, 3H), 2.15 – 2.06 (m, 2H). $^{13}$C NMR (100 MHz, $CDCl_3$) δ= 164.22, 146.98, 145.12, 139.20, 133.10, 132.20, 130.10, 128.59, 128.11, 120.23, 112.00, 69.51, 54.31, 28.43, 21.84, 21.56. $t_R$=8.2 min, 96%.

**2.4.14: 4-(4-(3-(tosyloxy) propyl)-1H-1,2,3-triazol-1-yl)pyridine (17)**

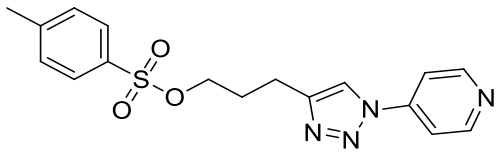

(34 mg, 19%). $^{1}$H NMR (400 MHz, DMSO-$d_6$) δ= 8.78 (d, *J* = 6.3 Hz, 2H), 8.74 (s, 1H), 7.92 (d, *J* = 6.4 Hz, 2H), 7.78 (d, *J* = 8.3 Hz, 2H), 7.43 (d, *J* = 8.0 Hz, 2H), 4.10 (t, *J* = 6.2 Hz, 2H), 2.73 (t, *J* = 7.5 Hz, 2H), 2.35 (s, 3H), 2.05 – 1.96 (m, 2H). $^{13}$C NMR (100 MHz, DMSO-$d_6$) δ= 151.60, 147.17, 144.86, 142.59, 132.28, 130.12, 127.57, 120.31, 113.32, 69.90, 27.59, 21.01, 20.83. $t_R$=0.49 min, 99%.

**2.4.15: 3-(4-(3-(tosyloxy) propyl)-1H-1,2,3-triazol-1-yl)pyridine (18)**

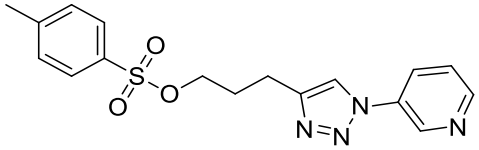

(53 mg, 30%). $^{1}$H NMR (400 MHz, DMSO-$d_6$) δ= 9.09 (d, *J* = 2.4 Hz, 1H), 8.68 (d, *J* = 3.5 Hz, 1H), 8.61 (s, 1H), 8.28 (d, *J* = 8.3 Hz, 1H), 7.78 (d, *J* = 8.2 Hz, 2H), 7.65 (dd, *J* = 8.3, 4.8 Hz, 1H), 7.44 (d, *J* = 8.1 Hz, 2H), 4.11 (t, *J* = 6.2 Hz, 2H), 2.73 (t, *J* = 7.5 Hz, 2H), 2.35 (s, 3H), 2.05 – 1.96 (m, 2H). $^{13}$C NMR (100 MHz, DMSO-$d_6$) δ= 149.46, 146.82, 144.87, 141.01, 133.32, 132.32, 130.13, 127.58, 124.60, 120.70, 69.97, 27.73, 21.02, 20.86. $t_R$=1.1 min, 96%.

**2.4.16: 2-(4-(3-(tosyloxy) propyl)-1H-1,2,3-triazol-1-yl)pyridine (19)**

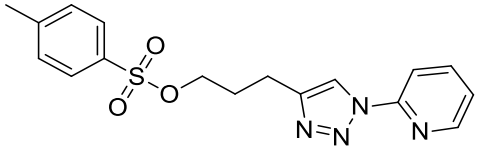

(47 mg, 27%). $^{1}$H NMR (400 MHz, DMSO-$d_6$) δ= 8.60 (d, *J* = 4.0 Hz, 1H), 8.53 (s, 1H), 8.10 (q, *J* = 16.1, 8.5 Hz, 2H), 7.77 (d, *J* = 7.9 Hz, 2H), 7.53 (t, *J* = 5.5 Hz, 1H), 7.43 (d, *J* = 8.0 Hz, 2H), 4.08 (t, *J* = 6.3 Hz, 2H), 2.73 (t, *J* = 7.6 Hz, 2H), 2.35 (s, 3H), 2.05 – 1.96 (m, 2H). $^{13}$C NMR (100 MHz, DMSO-$d_6$) δ= 148.87, 148.56, 146.53, 144.85, 140.04, 132.27, 130.13, 127.57, 124.07, 119.18, 113.46, 69.97, 27.65, 21.03, 20.84. $t_R$=0.36 min, 99%.

**2.4.17: 2-(4-(3-(tosyloxy) propyl)-1H-1,2,3-triazol-1-yl)thiazole (20)**

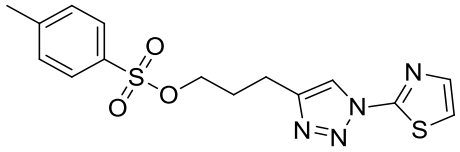

(69 mg, 57%). $^{1}$H NMR (400 MHz, DMSO-$d_6$) δ= 8.57 (s, 1H), 7.82 (dd, *J* = 3.5, 0.9 Hz, 1H), 7.80 – 7.74 (m, 3H), 7.44 (d, *J* = 8.0 Hz, 2H), 4.08 (t, *J* = 6.2 Hz, 2H), 2.73 (t, *J* = 7.5 Hz, 2H), 2.37 (s, 3H), 2.05 – 1.96 (m, 2H). $^{13}$C NMR (100 MHz, DMSO-$d_6$) δ= 156.80, 147.10, 144.88, 140.56, 132.25, 130.12, 127.57, 119.88, 119.54, 69.86, 27.46, 21.04, 20.73. $t_R$=0.35 min, 99%.

**2.4.18: Synthesis of carboxylic acid intermediate - Methyl 4-(4-(4-butanoic acid)-1H-1,2,3-triazol-1-yl)benzoate (22)**

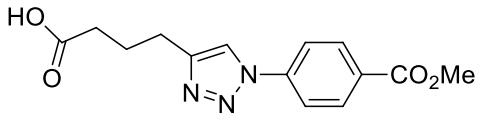

To a stirred solution of 4-azido benzoic acid (**21**, 1 eq) in 20 mL methanol was added 3 drops of concentrated sulfuric acid at room temperature. The reaction was then heated to reflux and stirred overnight at 90°C. Upon complete consumption of the acid, the solvent was removed under reduced pressure. The residue was then re-dissolved in ethyl acetate and washed 3 times with 1M NaOH. The organic layer was then dried over sodium sulphate, filtered, and concentrated *in vacuo* to afford the desired ester without further purification as a yellow solid (94%)**.** Methyl 4-azido benzoate (1 eq) was then dissolved in a THF/t-BuOH/ water (2:3:5) mixture, to which 5-hexynoic acid (1 eq), copper sulphate (0.3 M, 0.3

eq), and sodium ascorbate (0.1 M, 0.01 eq) were added. The reaction mixture was then stirred overnight at room temperature. Upon completion, the reaction mixture was partitioned between ethyl acetate and water and then washed 3 times with water. The organic layer was then dried over sodium sulphate, filtered and concentrated under reduced pressure to obtain the desired carboxylic acid intermediate **22** in 65% yield.

### 2.4.19: General synthetic procedure for the formation of amides (23-30)

To a stirred solution of carboxylic acid **22** (1 eq) in dichloromethane (10 mL) at room temperature was added the desired arylamine **1-5** (1.5 eq), 1-ethyl-3-(3-dimethylaminopropyl)carbodiimide (2.1 eq) and pyridine (2.1 eq) or 4-dimethylaminopyridine (2.1 eq). The reaction mixture was then stirred overnight at room temperature. Upon completion, the reaction mixture was partitioned between dichloromethane and water. The organic layer was then washed 3 times with water, dried over sodium sulphate, filtered and removed under reduced pressure. The desired amides were then purified using either column chromatography, preparative thin layer chromatography, or reverse phase column chromatography if necessary, to obtain amides (**23-30**) in low to modest yields (11-52%).

**2.4.20: Methyl 4-(4-(3-(*N*-3-pyridinylamido)propyl)-1H-1,2,3-triazol-1-yl)benzoate (23)**

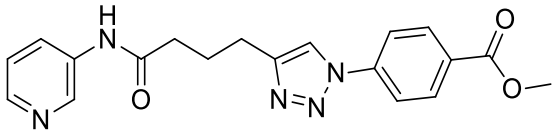

(28.9 mg, 46%). 1H NMR (400 MHz, DMSO-$d_6$) δ= 10.40 (s, 1H), 8.79 (d, *J* = 14.5 Hz, 2H), 8.22 (dd, *J* = 4.7, 1.5 Hz, 1H), 8.14 (d, *J* = 8.8 Hz, 2H), 8.11 – 8.04 (m, 3H), 7.31 (dd, *J* = 8.3, 4.7 Hz, 1H), 4.13 (q, *J* = 5.3 Hz, 1H), 3.89 (s, 3H), 3.16 (d, *J* = 5.2 Hz, 2H), 2.79 (t, *J* = 7.5 Hz, 2H), 2.06 – 1.96 (m, 2H). $^{13}$C NMR (100 MHz, DMSO-$d_6$) δ= 171.37, 165.31, 147.92, 143.90, 140.68, 139.91, 135.82, 130.92, 129.00, 125.88, 123.50, 120.43, 119.51, 52.31, 35.42, 24.46, 24.38. $t_R$=3.8 min, 96%.

**2.4.21: Methyl 4-(4-(3-(*N*-4-pyridinylamido)propyl)-1H-1,2,3-triazol-1-yl)benzoate (24)**

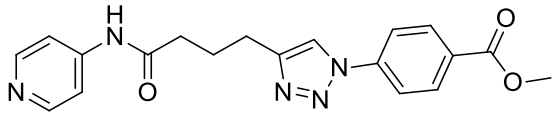

(23.9 mg, 38%). $^1$H NMR (400 MHz, DMSO-$d_6$) δ= 11.04 (s, 1H), 8.85 (s, 1H), 8.42 (d, *J* = 6.3 Hz, 2H), 8.12 (q, *J* = 17.7, 8.8 Hz, 4H), 7.72 (d, *J* = 6.5 Hz, 2H), 3.88 (s, 3H), 3.15 (s, 1H), 2.78 (t, *J* = 7.4 Hz, 2H), 2.54 (t, *J* = 7.5 Hz, 2H), 2.06 – 1.96 (m, 2H). $^{13}$C NMR (100 MHz, DMSO-$d_6$) δ= 172.05, 165.26, 149.87, 147.82, 145.84, 139.86, 130.85, 128.98, 120.38, 119.47, 52.23, 35.65, 24.37, 24.12. $t_R$=3.9 min, 97%.

**2.4.22: Methyl 4-(4-(3-(*N*-4-pyridinylamido)propyl)-1H-1,2,3-triazol-1-yl)benzoate (25)**

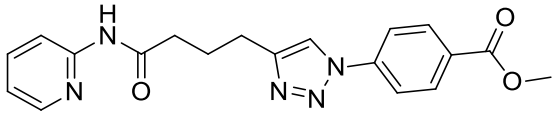

(39 mg, 31%). $^{1}$H NMR (400 MHz, $CDCl_3$) δ= 8.30 – 8.15 (m, 4H), 7.92 – 7.80 (m, 4H), 7.74 – 7.66 (m, 1H), 7.07 – 7.00 (m, 1H), 3.96 (s, 3H), 2.93 (t, *J* = 7.2 Hz, 2H), 2.54 (t, *J* = 7.2 Hz, 2H), 2.25 – 2.14 (m, 2H). $^{13}$C NMR (100 MHz, $CDCl_3$) δ= 171.99, 166.19, 155.22, 151.06, 148.33, 140.41, 131.54, 130.21, 119.97, 119.86, 119.47, 114.91, 52.64, 36.83, 24.98, 24.83, 18.66. $t_R$=5.0 min, 96%.

**2.4.23: Methyl 4-(4-(3-(*N*-2-thiazolamido)propyl)-1H-1,2,3-triazol-1-yl)benzoate (26)**

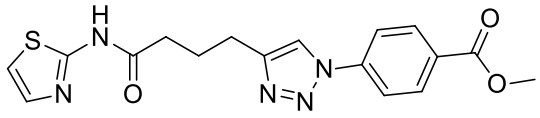

(66.5 mg, 52%). $^{1}$H NMR (400 MHz, $CDCl_3$) δ= 8.17 (d, *J* = 8.6 Hz, 2H), 7.85 (s, 1H), 7.80 (d, *J* = 8.6 Hz, 2H), 7.39 (d, *J* = 3.7 Hz, 1H), 6.93 (d, *J* = 3.6 Hz, 1H), 3.94 (s, 3H), 3.47 (s, 2H), 2.92 (t, *J* = 7.0 Hz, 2H), 2.63 (t, *J* = 7.1 Hz, 2H), 2.25 – 2.16 (m, 2H). $t_R$=2.3 min, 99%.

**2.4.24: Methyl 4-(4-(3-(*N*-2-methoxypyridinylamido)propyl)-1H-1,2,3-triazol-1-yl)benzoate (27)**

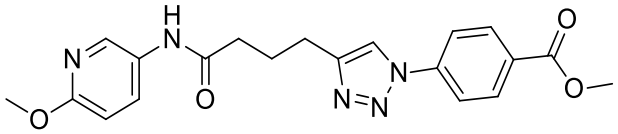

(32 mg, 23%).[1]H NMR (400 MHz, $CDCl_3$) δ= 8.51 (s, 1H, NH), 8.24 (s, 1H), 8.16 (d, *J* = 8.5 Hz, 2H), 7.93 (d, *J* = 8.9 Hz, 1H), 7.87 (s, 1H), 7.78 (d, *J* = 8.5 Hz, 2H), 6.68 (d, *J* = 8.9 Hz, 1H), 3.93 (s, 3H), 3.87 (s, 3H), 2.89 (t, *J* = 6.9 Hz, 2H), 2.47 (t, *J* = 7.0 Hz, 2H), 2.17 – 2.08 (m, 2H). [13]C NMR (100 MHz, $CDCl_3$) δ= 171.59, 166.08, 161.01, 148.46, 140.20, 138.57, 132.31, 131.55, 130.38, 129.18, 119.95, 119.63, 110.65, 53.75, 52.67, 36.06, 25.64, 24.35. $t_R$=4.8 min, 98%.

**2.4.25: Methyl 4-(4-(3-(*N*-2-oxazolamido)propyl)-1H-1,2,3-triazol-1-yl)benzoate (28)**

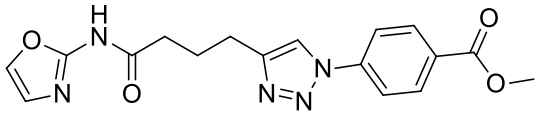

(20 mg, 16%). [1]H NMR (400 MHz, DMSO-$d_6$) δ= 11.11 (s, 1H), 8.76 (s, 1H), 8.16 (d, *J* = 8.6 Hz, 2H), 8.07 (d, *J* = 8.6 Hz, 2H), 7.84 (s, 1H), 7.07 (s, 1H), 3.89 (s, 3H), 3.29 (t, 2H), 2.76 (t, *J* = 7.5 Hz, 2H), 2.02 – 1.93 (m, 2H). [13]C NMR (100 MHz, DMSO-$d_6$) δ= 165.38, 153.24, 147.91, 139.96, 135.92, 130.99, 129.04, 126.54, 120.50, 119.59, 99.52, 52.39, 34.63, 24.35, 24.00. $t_R$=0.45 min, 99%

**2.4.26: Methyl 4-(4-(3-(*N*-5-1,2,4-thiadiazolamido)propyl)-1H-1,2,3-triazol-1-yl)benzoate (29)**

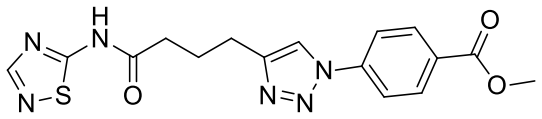

(29 mg, 23%). $^{1}$H NMR (400 MHz, DMSO-$d_6$) δ= 12.94 (s, 1H), 8.77 (s, 1H), 8.44 (s, 1H), 8.15 (d, *J* = 8.7 Hz, 2H), 8.06 (d, *J* = 8.8 Hz, 2H), 3.89 (s, 3H), 2.79 (t, *J* = 7.5 Hz, 2H), 2.65 (t, *J* = 7.3 Hz, 2H), 2.10 – 2.00 (m, 2H). $^{13}$C NMR (100 MHz, DMSO-$d_6$) δ= 174.80, 172.94, 165.37, 158.46, 147.70, 139.94, 130.99, 129.05, 120.57, 119.57, 52.39, 33.77, 24.30, 23.83. $t_R$=1.3 min, 99%.

**2.4.27: Methyl 4-(4-(3-(*N*-4-pyrimidinylamido)propyl)-1H-1,2,3-triazol-1-yl)benzoate (30)**

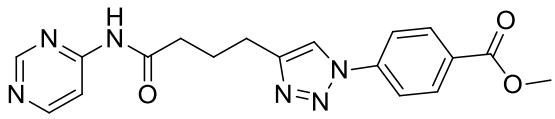

(14 mg, 11%). $^{1}$H NMR (400 MHz, DMSO-$d_6$) δ= 10.89 (s, 1H), 8.85 (s, 1H), 8.76 (s, 1H), 8.62 (d, *J* = 5.7 Hz, 1H), 8.15 (d, *J* = 8.3 Hz, 2H), 8.09 – 8.03 (m, 3H), 3.89 (s, 3H), 2.77 (t, *J* = 7.4 Hz, 2H), 2.54 (t, *J* = 7.3 Hz, 2H), 2.04 – 1.95 (m, 2H). $^{13}$C NMR (100 MHz, DMSO-$d_6$) δ= 173.24, 165.37, 158.26, 158.18, 157.56, 147.89, 139.95, 130.99, 129.03, 120.52, 119.57, 109.73, 52.39, 35.44, 24.38, 24.05. $t_R$=0.46 min, 99%

### 2.5: Procedure for protein thermal shift assay

The thermal shift assay utilized a MicroAmp 96-well plate and 20 μM of gankyrin in buffer containing 8x Sypro Orange (Applied Biosystems). 5 mM of each compound were obtained from a DMSO stock, and a concentration of 300 μM was established with DMSO at a concentration of 5% vol/vol for each compound. Three trials were performed for each compound. Gankyrin unfolding was performed at a temperature range of 15 ˚C to 65 ˚C. SYPRO Orange fluorescence was tracked as a function of temperature in order to generate melting curves. The inflection point of the sigmoid is taken to be the melting temperature $T_m$. The difference in melting temperature ($\Delta T_m$) indicates the absolute value of difference between the melting temperature of gankyrin only and the melting temperature of gankyrin with molecule ligand bound. This difference in melting temperature indicates binding affinity as the greater the $\Delta T_m$, the greater the binding affinity.

## 3. Results and discussion

### 3.1: Chemistry

#### 3.1.1: Synthesis of cjoc42 derivatives (16-20)

Scheme 1[a]

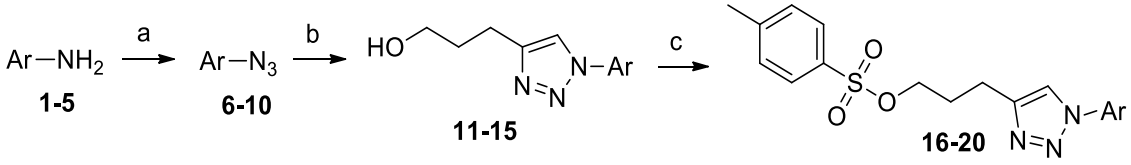


[a]Reagents: (a) HCl, $NaNO_2$, $NaN_3$. (b) 4-pentynol, sodium ascorbate, $CuSO_4$, THF, $H_2O$, tBuOH. (c) CH2Cl2, DMAP, TEA, p-tosyl Chloride. Ar = Various aromatic heterocycles.

The synthesis of cjoc42 derivatives **16-20** (**Scheme 1**) was initiated with the diazotisation of various aromatic heterocyclic amines (**1-5**) followed by addition of sodium azide to generate substituted azido intermediates **6-10**. The obtained azido intermediates were then involved in a copper-catalysed alkyne-azide cycloaddition (CuAAC) with 4-pentyn-1-ol in the presence of copper sulphate and sodium ascorbate to afford triazole intermediates **11-15** in modest yields (3%-42%) over 2 steps. These intermediates were then subjected to a nucleophilic substitution reaction with *p*-tosyl chloride in the presence of trimethylamine and 4-dimethylaminopyridine to generate various cjoc42 derivatives **16-20** in modest to good yields (19%-57%).

### 3.1.2: Synthesis of amide bond derivatives (23-30)

Scheme 2[a]

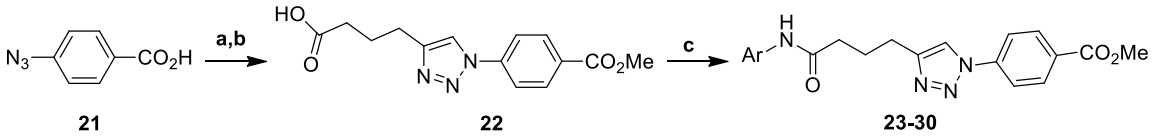


[a]Reagents: (a) $H_2SO_4$, MeOH; (b) 5-hexynoic acid, sodium ascorbate, $CuSO_4$, THF, $H_2O$, tBuOH. (c) Pyridine, EDCI, Ar-$NH_2$. Ar = Various aromatic heterocycles.

The synthesis of cjoc42 derivatives **23-30** (**Scheme 2**) was initiated with the acid-catalysed methyl esterification of 4-azidobenzoic acid **21** to generate methyl 4-azidobenzoate. This intermediate then underwent a copper-catalysed alkyne-azide cycloaddition (CuAAC) with 5-hexynoic acid in the presence of copper sulphate and sodium ascorbate to afford triazole intermediate **22** in good yield (70%). This intermediate was then reacted with various arylamines in the presence of 1-Ethyl-3-(3-dimethylaminopropyl)carbodiimide and pyridine or 4-Dimethylaminopyridine to generate amide-based cjoc42 derivatives **23-30** in varying yields (11-52%).

### 3.2: Thermal shift assay

All cjoc42 derivatives (**16-20**, **23-25**, **27**) were evaluated in a protein thermal shift assay in order to determine their relative gankyrin binding and compare them to cjoc42. The protein thermal shift assay determines the melting temperature of a protein ($T_m$), which is the temperature at which the protein denatures. At the melting point of a protein, it loses its quaternary, tertiary and secondary structure. This exposes the protein's hydrophobic residues which in turn bind to the hydrophobic fluorescent dye (SYPRO orange). The fluorescence intensity is an indicator of the different stages of unfolding during the melting process. The melting temperature of a protein will be shifted when it binds effectively with a ligand as compared to a protein with no ligand bound. This shift in melting temperature ($\Delta T_m$) indicates if a ligand could be more or less effective in binding, where the larger the $\Delta T_m$, the more effective a ligand binds to the protein.

To evaluate the relative gankyrin binding affinity of our cjoc42 derivatives, the $\Delta T_m$ of cjoc42 bound to gankyrin was first determined, then the $\Delta T_m$ of our synthesised cjoc42 derivatives (**16-20**, **23-25**, **27)** were determined. The $\Delta T_m$ of each cjoc42 derivative was then be compared to cjoc42 and ranked comparatively. All the synthesised cjoc42 derivatives (**16-20**, **23-25**, **27**) with their respective $\Delta T_m$ are shown in **Figure 6** and **Figure 7** along with the $\Delta T_m$ value of cjoc42.

Cjoc42 derivatives **16-20** (**Figure 6**) exhibit a range of $\Delta T_m$ values, indicating a range in relative binding affinities for gankyrin. Replacing the methyl benzoate ester of cjoc42 with various heteroaromatic systems **16-20** all resulted in slightly enhanced gankyrin binding affinity as compared to cjoc42. This enhanced affinity could be due to improved interactions with W46 and $R_{41}$ at the binding site of gankyrin (**Figure 5,** Top).

An enhanced interaction with R41 could indicate an enhanced hydrogen bonding compared to cjoc42. An interaction with W46 (**Figure 5**, Top) involves pi-pi stacking between the non-polar indole of tryptophan and the heteroaromatic systems of these cjoc42 derivatives.

For compounds **23-30**, the sulfonate ester group of cjoc42 was replaced with an amide group, which had previously demonstrated a similar binding affinity to cjoc42. In addition, compounds **23-30** also replaced the tolyl group of cjoc42 with various heteroaromatic systems. Unfortunately, most of these compounds exhibited a decrease in gankyrin binding affinity as compared to cjoc42. Compound **24** was the one exception by exhibiting very similar gankyrin binding affinity as compared to cjoc42. This data suggests that the introduction of more polar groups present in the heteroaromatic systems could negatively affect an interaction with $W_{74}$. The non-polar indole of the $W_{74}$ amino acid side chain could be the reason that there is a decrease in affinity between gankyrin and cjoc42 derivatives **23**, **25** and **27**.

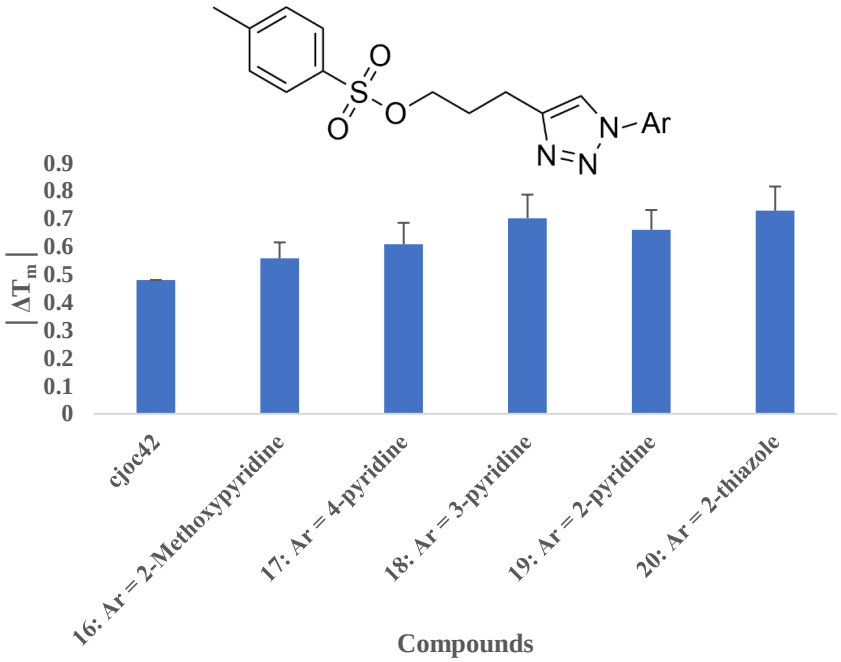


**Figure 6**. Thermal shift values for cjoc42 derivatives **16-20** for evaluation of cjoc42 derivatives. Absolute values of $\Delta T_m$ are plotted.

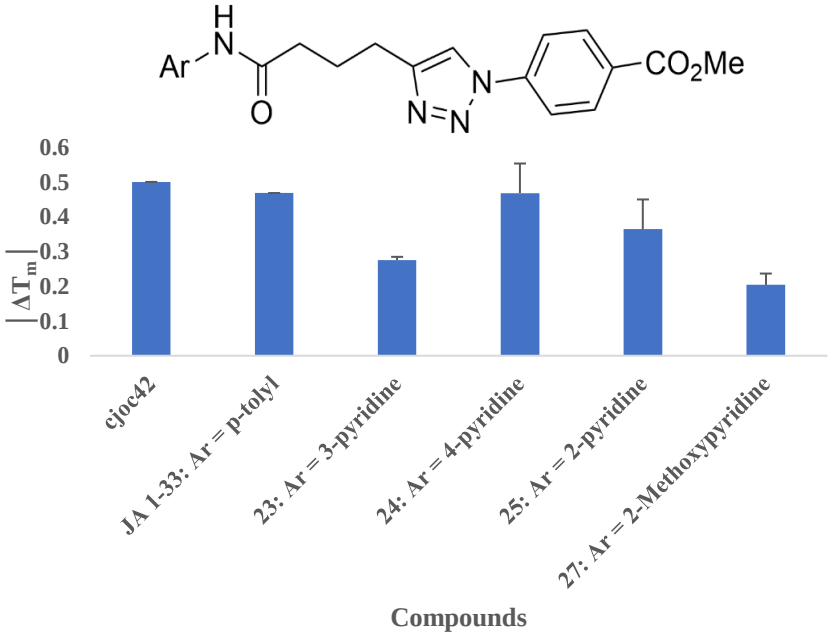


**Figure 7**. Thermal shift values for cjoc42 derivatives **23-25**, **27** for evaluation of cjoc42 derivatives. Absolute values of $\Delta T_m$ are plotted.

Overall, compounds **16-20** exhibited improved gankyrin binding affinities as compared to cjoc42; whereas compounds **23-27** displayed similar or decreased gankyrin binding affinities as compared to cjoc42.

**4. ClogP of synthesised derivatives**

It has been previously observed that cjoc42 possesses poor water solubility, which could impair its ability to reach the desired target without precipitating. Therefore, it was sought to increase the hydrophilicity of the cjoc42 scaffold to enhance its bioavailability. The hydrophobicity and subsequent hydrophilicity of compounds **16-20, 23-30** could be predicted from the clogP values. logP is the partition coefficient of a compound between n-octanol and water; the logP of a compound indicates the ratio of its solubility in two solvents that are immiscible. ClogP is the calculated logP and it can be predicted by software such as ChemDraw, and the algorithm is developed by Biobyte. It is based on a programmable method of dissecting a solute structure into specific fragments. The program accesses values for the fragments which are measured in any one of five bonding environments which can account for differences in various bond types (e.g., aliphatic, benzyl, vinyl, styryl or aromatic). If the fragment is found, but not in the desired bond environment, it estimates the difference and reports it as 'derived'. It then sums fragment values and makes important interaction corrections when fragments occur in proximity to one another. If the desired fragment structure is absent from the database, the program calculates it using a method (FRAGCALC) which examines all atoms and their neighbors and uses an equation based on eleven possible parameters which can raise or lower their hydrophobic contribution.[49] Compounds that have high clogP values suggest they are highly hydrophobic and poorly hydrophilic, whereas low clogP values indicate the compounds are more water soluble and less lipid soluble. Compounds with desired drug-likeness should have a clogP value no greater than 5. ClogP is important to the biological properties of the proposed compounds since they need to be hydrophilic enough to stay

solubilized in the bloodstream which is aqueous, while also being hydrophobic enough to pass through the phospholipid bilayer and effectively delivered to the cell. Therefore, balancing the hydrophobicity and hydrophilicity is crucial and was important to the design of our cjoc42 derivatives.

LogP values can be powerful predictors of drug efficacy. When the logP is calculated, it typically is similar to its actual logP, however, it may deviate to some degree as well. For example, the logP value of ibuprofen is 3.97[50], where clogP predicted from ChemDraw is 3.68. This shows the 2 numbers to be similar, but there is a slight difference between published logP and predicted clogP. clogP could be an indicator of drug efficacy when comparing the clogP values, however, the efficacy of drugs has to be demonstrated in controlled clinical trials by statistical evaluation.

Cjoc42 has a clogP value of 3.4 as shown in Table 1, and a proposed compound 23 has a clogP value of 2.57, which indicates a more water-soluble compound from its predicted properties. From the proposed compounds **23-25**, it would be reasonable to predict that they all have a lower clogP value than cjoc42 due to the presence of multiple heteroatoms present in the amide bond and heteroaromatic system.

**Table 1.** Thermal Shift Values and clogP Values of cjoc42 Derivatives **16-20** and **23-30**.

| Compound | Structure | Thermal shift values | clogP |
|---|---|---|---|
| cjoc42 | 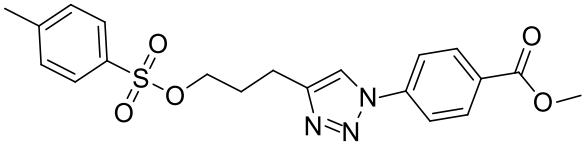 | 0.500 (±0.01) | 3.40 |
| JA 1-33 | 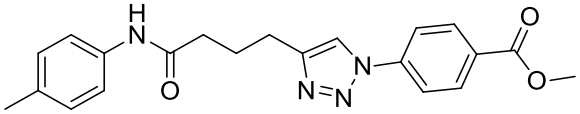 | 0.480 (±0.02) | 3.74 |
| 16 | 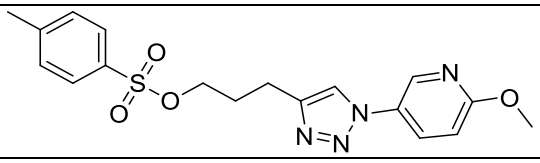 | 0.558 (±0.06) | 3.09 |
| 17 | 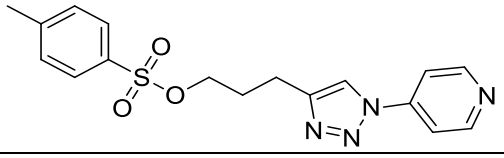 | 0.608 (±0.08) | 2.33 |
| 18 | 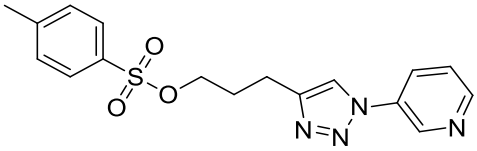 | 0.702 (±0.08) | 2.33 |
| 19 | 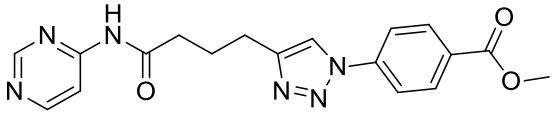 | 0.660 (±0.07) | 2.33 |
| 20 | 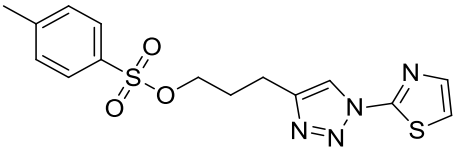 | 0.729 (±0.09) | 2.37 |
| 23 | 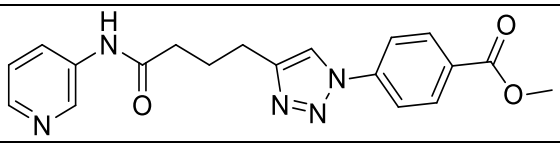 | 0.275 (±0.01) | 2.57 |
| 24 | 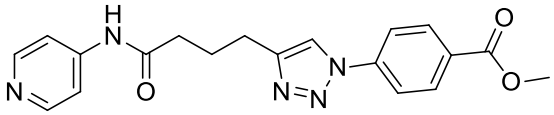 | 0.468 (±0.09) | 2.57 |
| 25 | 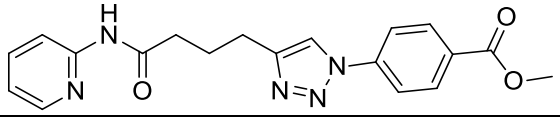 | 0.364 (±0.09) | 2.57 |
| 26 | 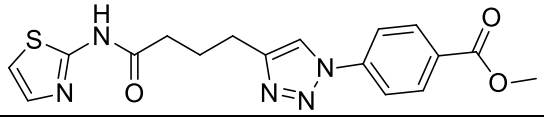 | N/T | 2.7 |

| Compound | Structure | Thermal shift values | clogP |
|---|---|---|---|
| 27 | 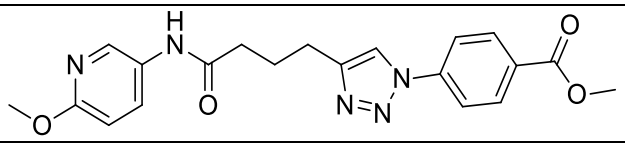 | 0.204 (±0.03) | 3.41 |
| 28 | 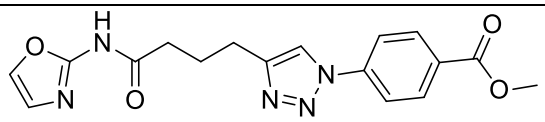 | N/T | 1.74 |
| 29 | 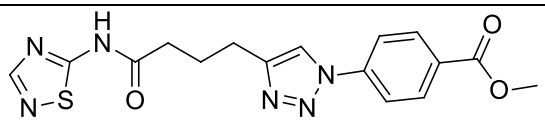 | N/T | 2.03 |
| 30 | 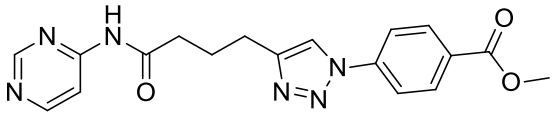 | N/T | 1.90 |

Compounds **23-30** showed a more significant decrease in clogP values compared to cjoc42 than compounds **16-20**. This could due to that fact that the benzoate ester is generally more hydrophobic than the various heteroaromatic replacements. Compounds **19, 23-26, 28-30** also has lower clogP value than cjoc42, which could still be considered as further research basis since these compounds potentially possesses greater metabolic stability from their amide bond replacement of the sulphonate ester bond.

Overall, replacing the methyl benzoate and tolyl groups of cjoc42 with various heteroaromatic groups resulted in a decrease in clogP which should improve the aqueous solubility of the synthesised compounds as desired.

## 5. Conclusion

A total of 14 cjoc42 derivatives were synthesised. with 5 derivatives (**16**-**20**) replaced the methyl benzoate of cjoc42 with heteroaromatic groups, and 8 derivatives (**23**-**30**) replaced the sulfonate ester of cjoc42 with an amide bond as well as the tolyl group of cjoc42 with various heteroaromatic groups. Replacing the methyl benzoate of cjoc42 with heteroaromatic groups focused on optimising hydrogen bonding with $R_{41}$ (**Figure 5**, Top), and improving the aqueous solubility of the compounds. Biophysical analysis in a protein thermal shift showed that replacing the methyl benzoate of cjoc42 with a 3-pyridine (**23**), 4-pyridine (**24**) or 2-pyridine (**25**) group slightly improved gankyrin binding affinity as compared to cjoc42. These 3 derivatives are also predicted to display enhanced water solubility with a clogP of 2.57 for all three of them, where cjoc42 has a clogP of 3.4. Derivatives **23**-**25**, **27** did not show enhanced gankyrin binding as compared to cjoc42, however, but they did predict enhanced water solubility due to their lower clogP values as compared to cjo42. These findings demonstrate that replacing the methyl benzoate of cjoc42 with various aromatic heterocycles can improve water solubility while also improving gankyrin binding, and that replacing the sulfonate ester of cjoc42 with an amide bond as well as the tolyl group of cjoc42 with various heteroaromatic groups could improve water solubility but not gankyrin binding affinity.

## 6. Future directions

Going forward, cjoc42 derivatives **16-20**, **23-25**, **27** will be evaluated in other biological assays for their ability to inhibit cancer cell migration, proliferation and metastasis in gankyrin-overexpressing cancer cell lines. Specifically, these compounds will be evaluated in hepatoblastoma cell lines (HepG2 and Hep3B), non-small cell lung cancer cell lines (A549) as well as breast cancer cell lines (MDA-MB-231), to observe their ability to inhibit cell proliferation and migration. Further optimization of the cjoc42 scaffold will be conducted by combining the optimal functional groups at different position in various cjoc42 derivatives for enhanced gankyrin binding and anti-cancer activity. Secondary biophysical assays will be included to further confirm gankyrin binding affinity, such as isothermal titration calorimetry (ITC) and surface plasmon resonance (SPR). Cjoc42 derivatives with improved efficacy in cell-based assays could ultimately prove to be future anti-cancer therapeutic agents.

## 7. Appendix

### 7.1: 1H and C13 NMR Spectra for intermediates (11-15)

#### 7.1.1: 3-(4-(3-hydroxypropyl)-1*H*-1,2,3-triazol-1-yl)pyridine (11)

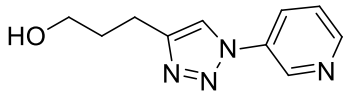


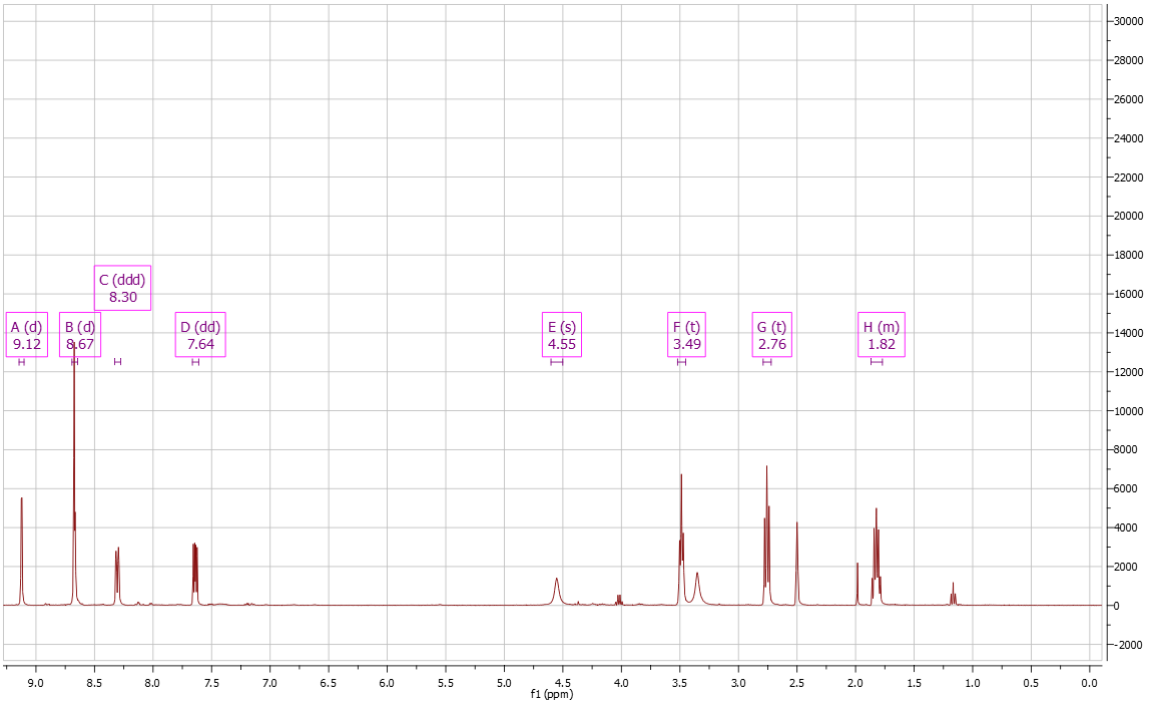

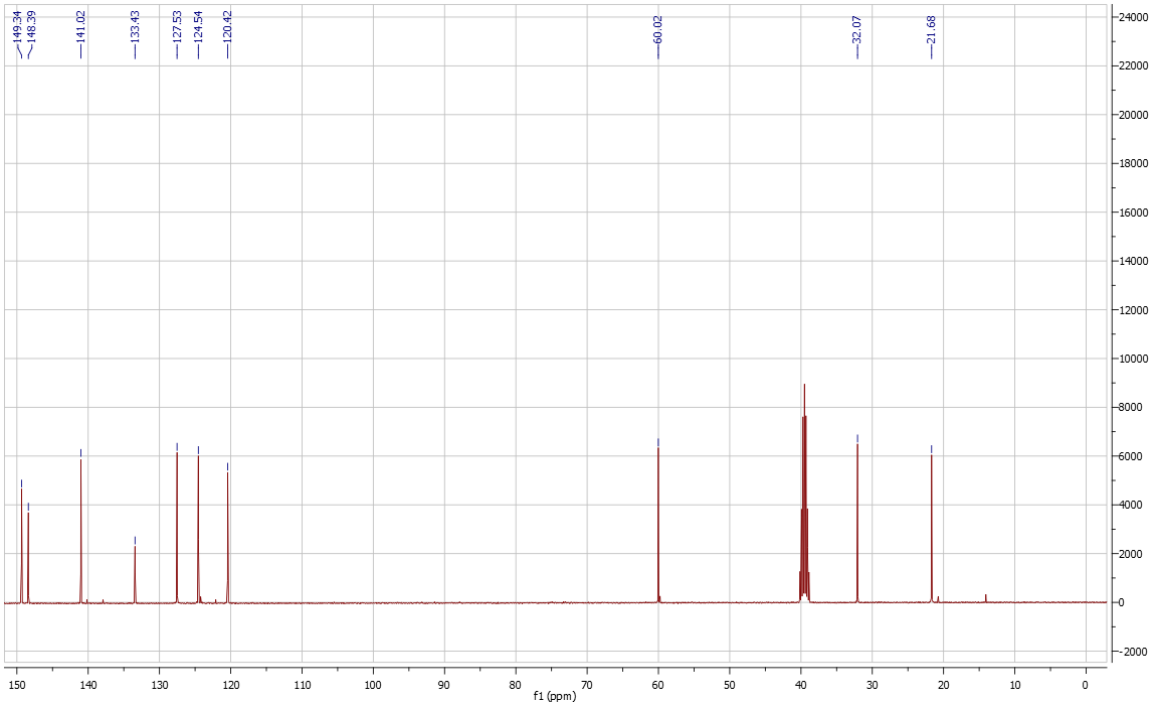


(371mg, 22%). $^{1}$H NMR (400 MHz, DMSO-$d_6$) δ= 9.12 (d, *J* = 2.5 Hz, 1H), 8.67 (d, 2H), 8.30 (ddd, *J* = 8.3, 2.5, 1.4 Hz, 1H), 7.64 (dd, *J* = 8.3, 4.8 Hz, 1H), 4.55 (s, 1H), 3.49 (t, *J* = 6.3 Hz, 2H), 2.76 (t, 2H), 1.87 – 1.77 (m, 2H). $^{13}$C NMR (100 MHz, DMSO-$d_6$) δ= 149.34, 148.39, 141.02, 133.43, 127.53, 124.54, 120.42, 60.02, 32.07, 21.68.

### 7.1.2: 4-(4-(3-hydroxypropyl)-1*H*-1,2,3-triazol-1-yl)pyridine (12)

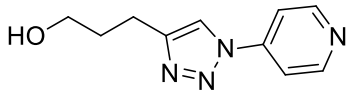


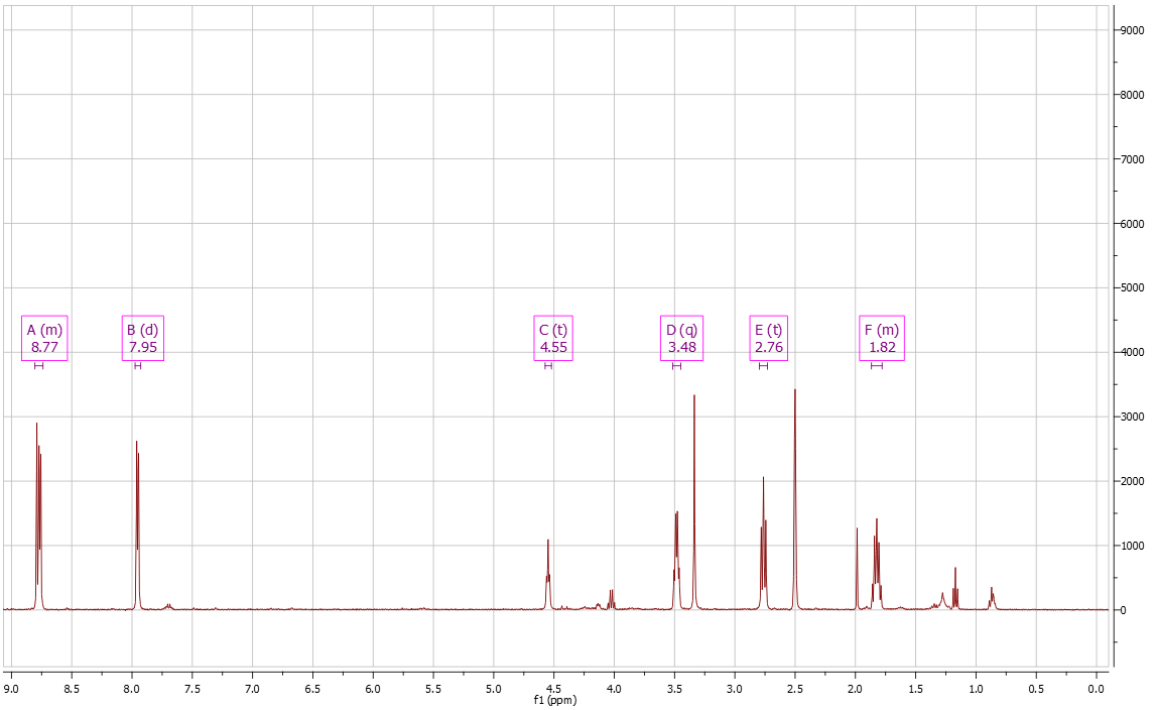


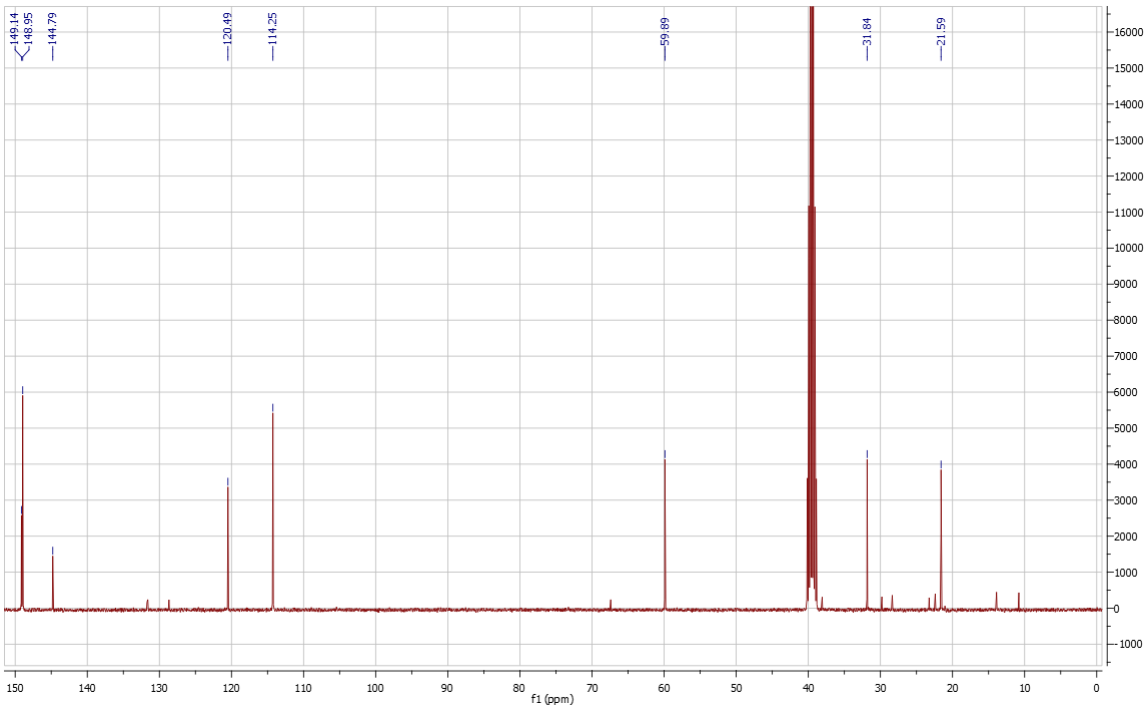

(314mg, 42%). $^{1}$H NMR (400 MHz, DMSO-$d_6$) δ= 8.80 – 8.74 (m, 3H), 7.95 (d, *J* = 6.3 Hz, 2H), 4.55 (t, *J* = 5.0 Hz, 1H), 3.48 (m, 2H), 2.76 (t, *J* = 7.7 Hz, 2H), 1.87 – 1.78 (m, 2H). $^{13}$C NMR (100 MHz, DMSO-$d_6$) δ= 149.14, 148.95, 144.79, 120.49, 114.25, 59.89, 31.84, 21.59.

### 7.1.3: 2-(4-(3-hydroxypropyl)-1*H*-1,2,3-triazol-1-yl)thiazole (13)

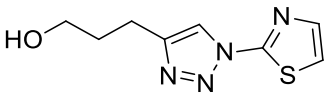


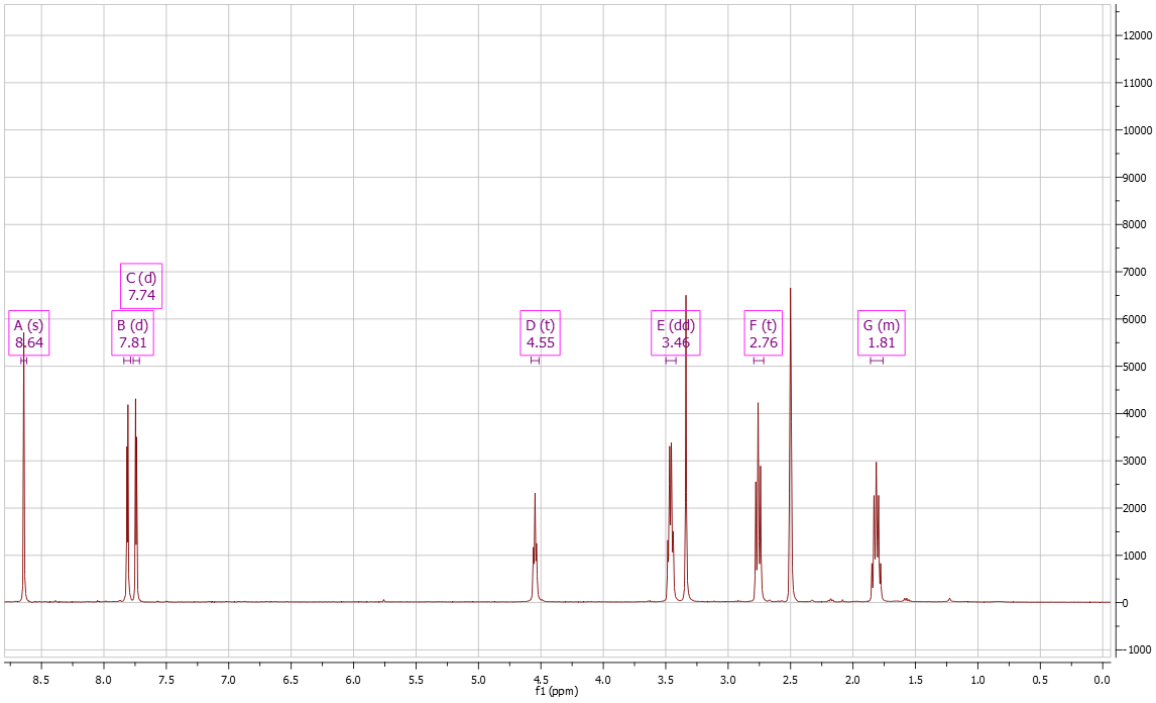

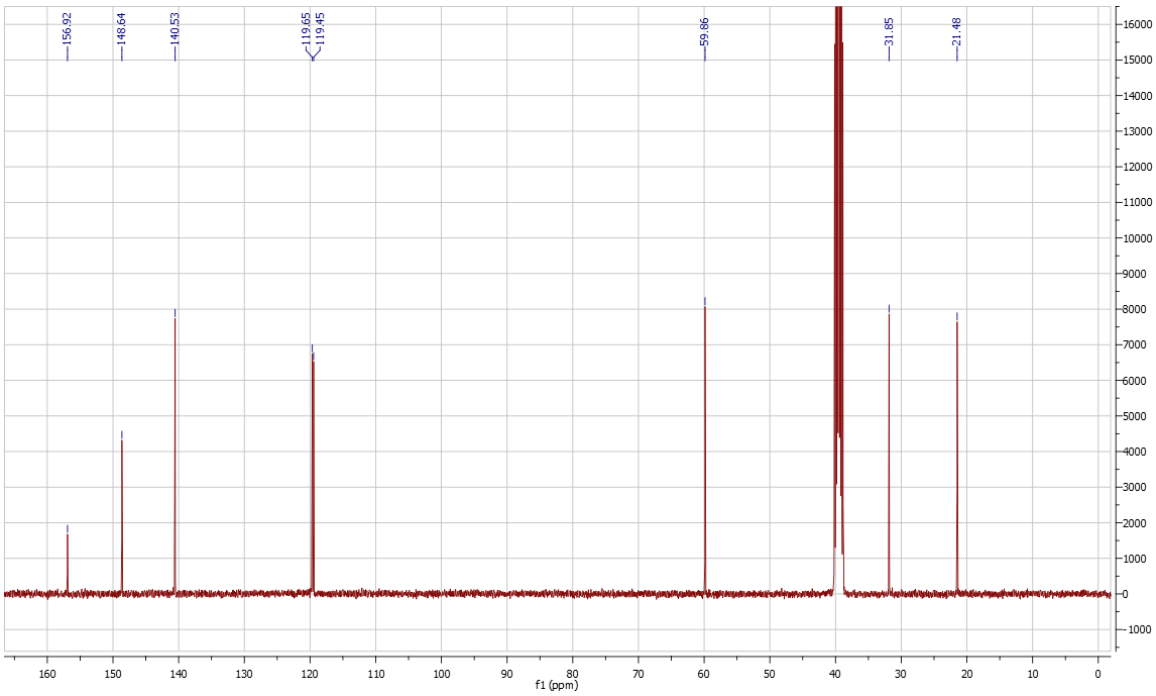


(76mg, 3%). $^{1}$H NMR (400 MHz, DMSO-$d_6$) δ= 8.64 (s, 1H), 7.81 (d, *J* = 3.4 Hz, 1H), 7.74 (d, *J* = 3.4 Hz, 1H), 4.55 (t, *J* = 5.1 Hz, 0H), 3.46 (q, *J* = 11.7, 6.0 Hz, 2H), 2.76 (t, *J* = 7.7 Hz, 2H), 1.86 – 1.76 (m, 2H). $^{13}$C NMR (101 MHz, DMSO-$d_6$) δ 156.92, 148.64, 140.53, 119.65, 119.45, 59.86, 31.85, 21.48.

### 7.1.4 2-(4-(3-hydroxypropyl)-1*H*-1,2,3-triazol-1-yl)pyridine (14)

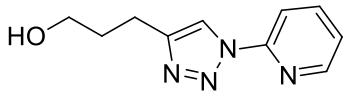


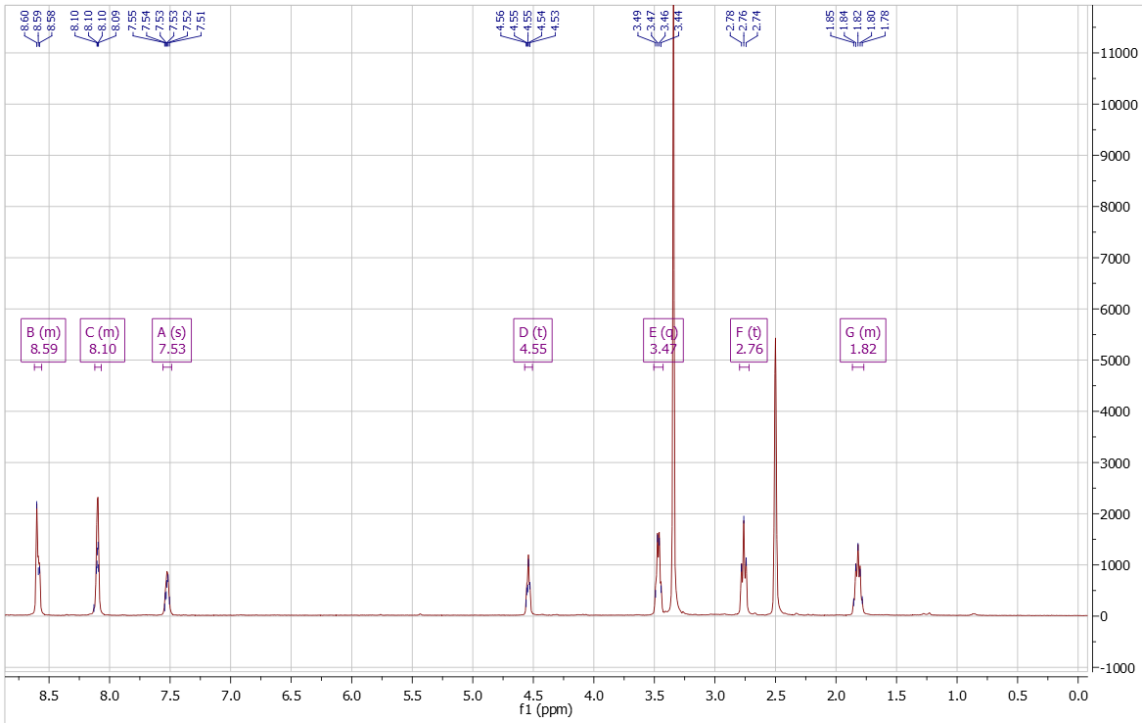


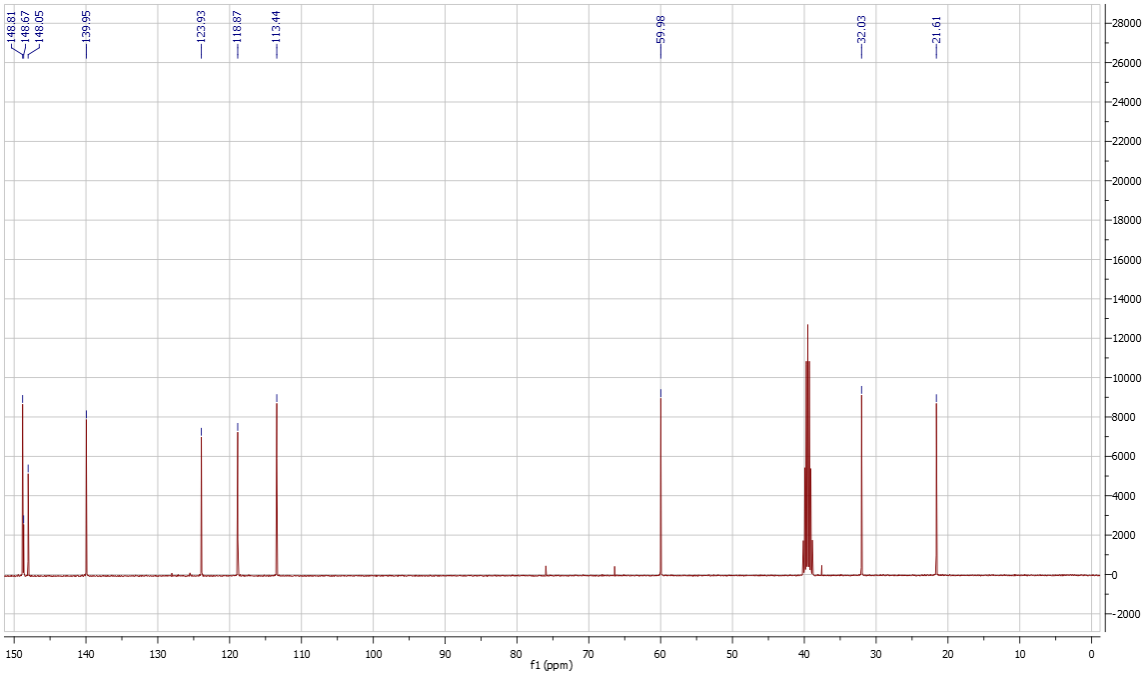

(177mg, 10%). $^{1}$H NMR (400 MHz, DMSO-$d_6$) δ 8.62 – 8.56 (m, 2H), 8.12 – 8.07 (m, 2H), 7.53 (s, 1H), 4.55 (t, *J* = 5.1 Hz, 1H), 3.47 (q, *J* = 11.4, 6.2 Hz, 2H), 2.76 (t, *J* = 7.7 Hz, 2H), 1.86 – 1.77 (m, 2H). $^{13}$C NMR (101 MHz, DMSO-$d_6$) δ 148.81, 148.67, 148.05, 139.95, 123.93, 118.87, 113.44, 59.98, 32.03, 21.61.

### 7.2: 1H and C13 NMR for Sulphonate Esters (16-20)

#### 7.2.1: 2-(4-(3-(tosyloxy) propyl)-1H-1,2,3-triazol-1-yl)methoxypyridine (16)

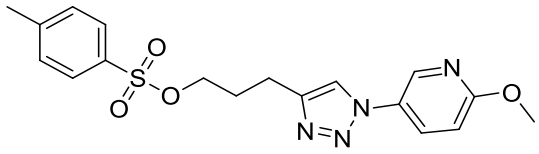

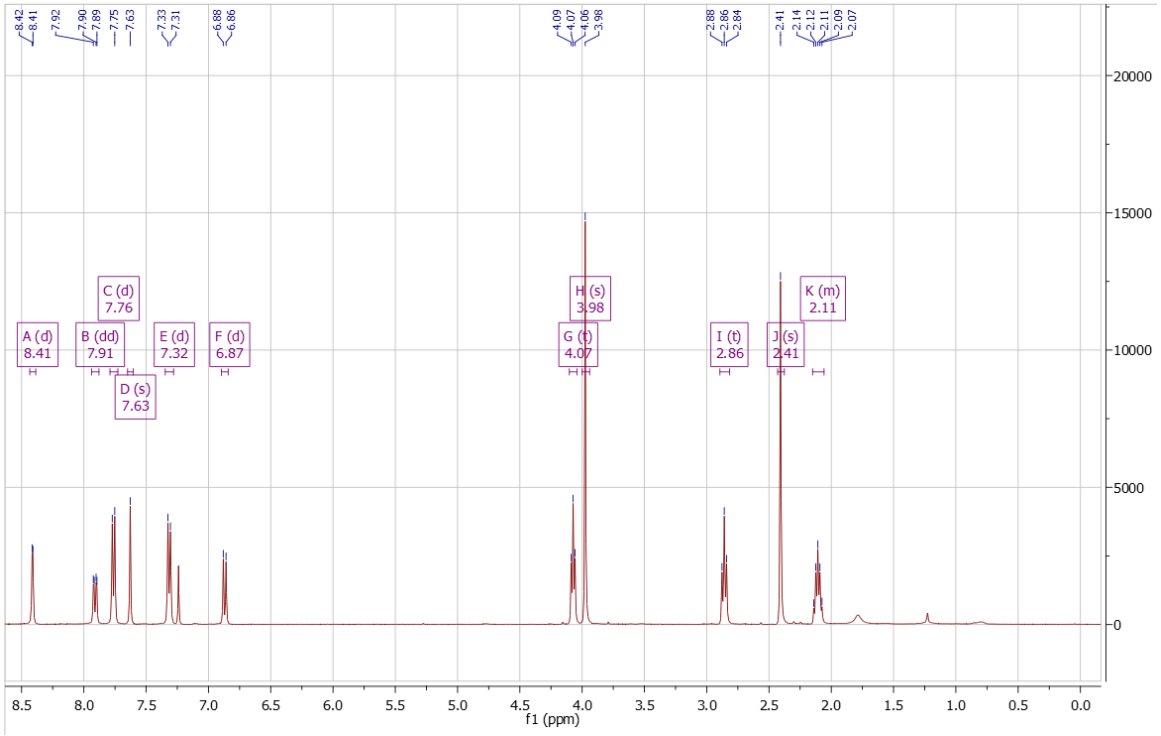

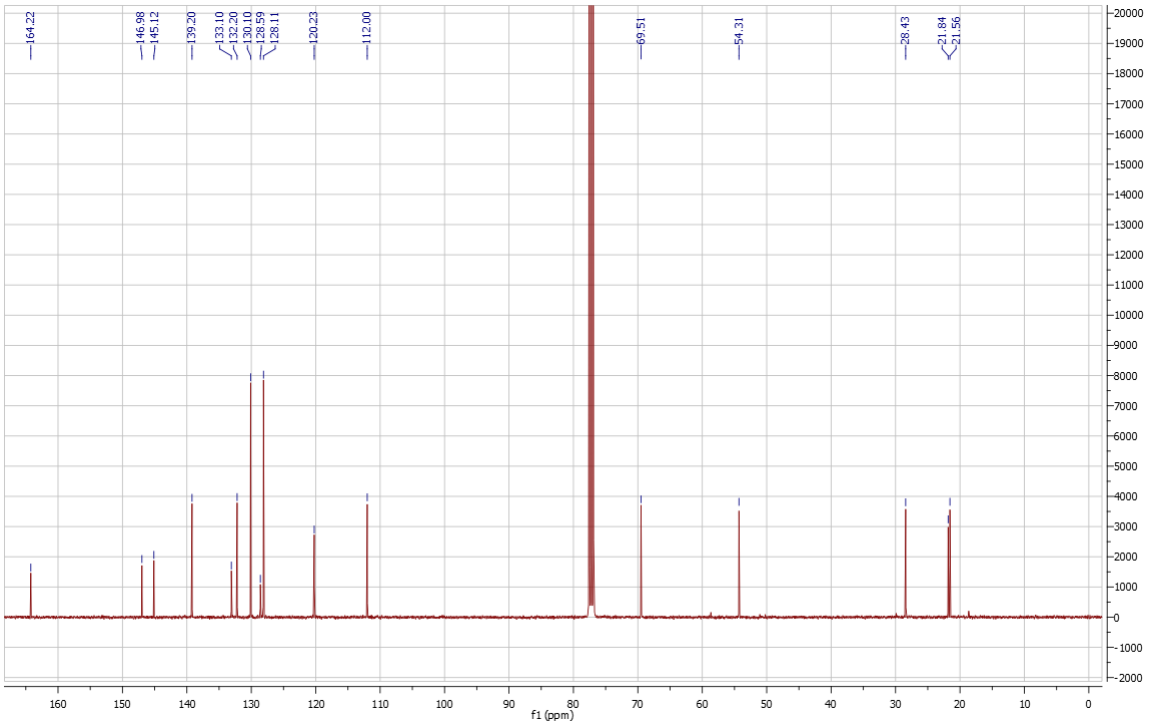


(22 mg, 13%). $^{1}$H NMR (400 MHz, $CDCl_3$) δ= 8.41 (d, *J* = 2.8 Hz, 1H), 7.91 (dd, *J* = 8.9, 2.8 Hz, 1H), 7.76 (d, *J* = 8.0 Hz, 2H), 7.63 (s, 1H), 7.32 (d, *J* = 8.0 Hz, 2H), 6.87 (d, *J* = 8.9 Hz, 1H), 4.07 (t, *J* = 6.0 Hz, 2H), 3.98 (s, 3H), 2.86 (t, *J* = 7.3 Hz, 2H), 2.41 (s, 3H), 2.15 – 2.06 (m, 2H). $^{13}$C NMR (100 MHz, $CDCl_3$) δ= 164.22, 146.98, 145.12, 139.20, 133.10, 132.20, 130.10, 128.59, 128.11, 120.23, 112.00, 69.51, 54.31, 28.43, 21.84, 21.56. $t_R$=8.2 min, 96%.

### 7.2.2: 4-(4-(3-(tosyloxy) propyl)-1H-1,2,3-triazol-1-yl)pyridine (17)

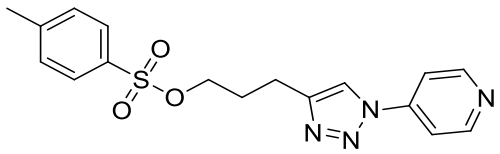

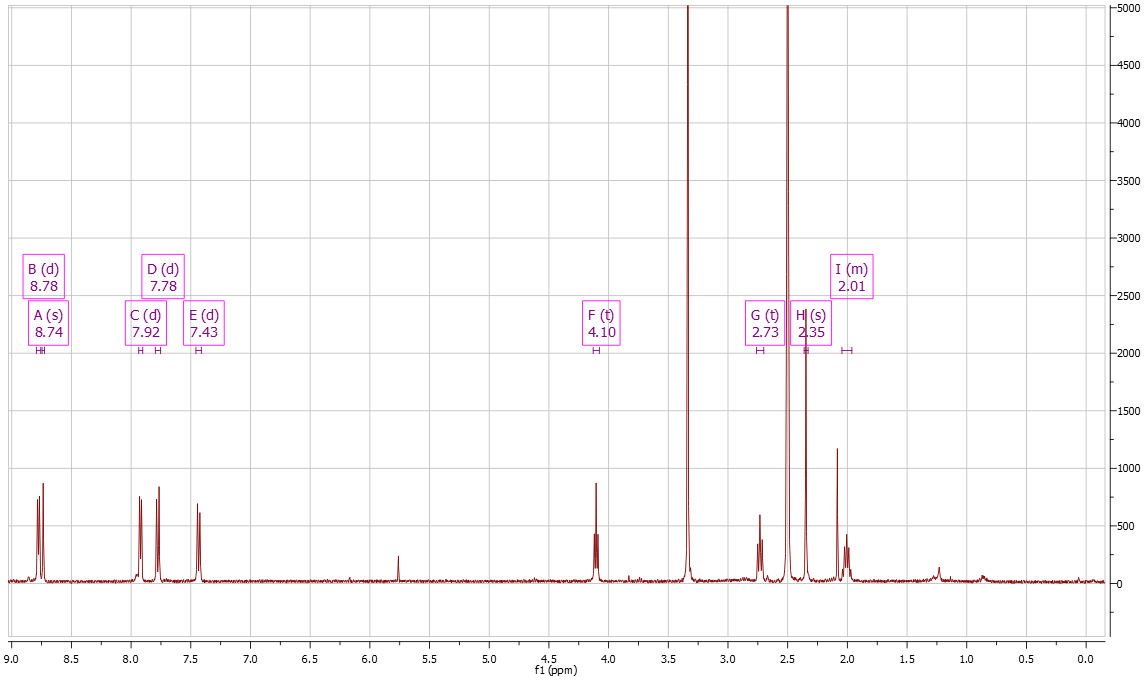


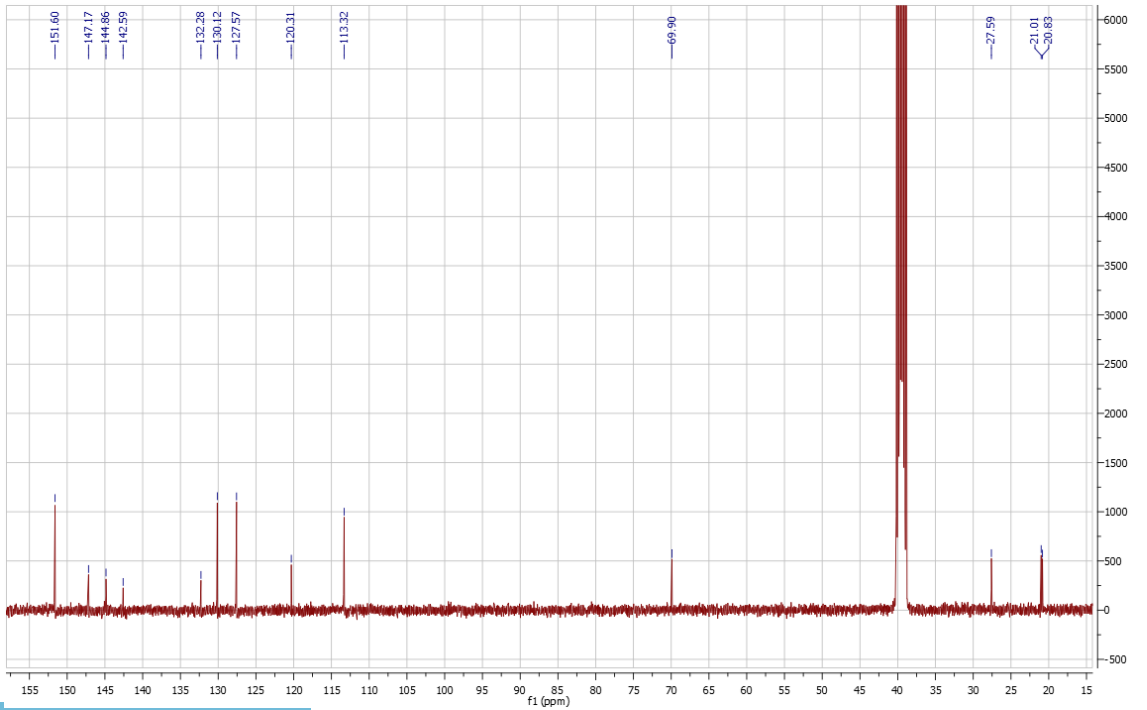

(34 mg, 19%). $^{1}$H NMR (400 MHz, DMSO-$d_6$) δ= 8.78 (d, *J* = 6.3 Hz, 2H), 8.74 (s, 1H), 7.92 (d, *J* = 6.4 Hz, 2H), 7.78 (d, *J* = 8.3 Hz, 2H), 7.43 (d, *J* = 8.0 Hz, 2H), 4.10 (t, *J* = 6.2 Hz, 2H), 2.73 (t, *J* = 7.5 Hz, 2H), 2.35 (s, 3H), 2.05 – 1.96 (m, 2H). $^{13}$C NMR (100 MHz, DMSO-$d_6$) δ= 151.60, 147.17, 144.86, 142.59, 132.28, 130.12, 127.57, 120.31, 113.32, 69.90, 27.59, 21.01, 20.83. $t_R$=0.49 min, 99%.

### 7.2.3: 3-(4-(3-(tosyloxy) propyl)-1H-1,2,3-triazol-1-yl)pyridine (18)

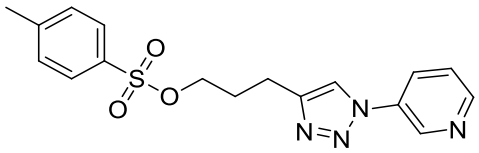

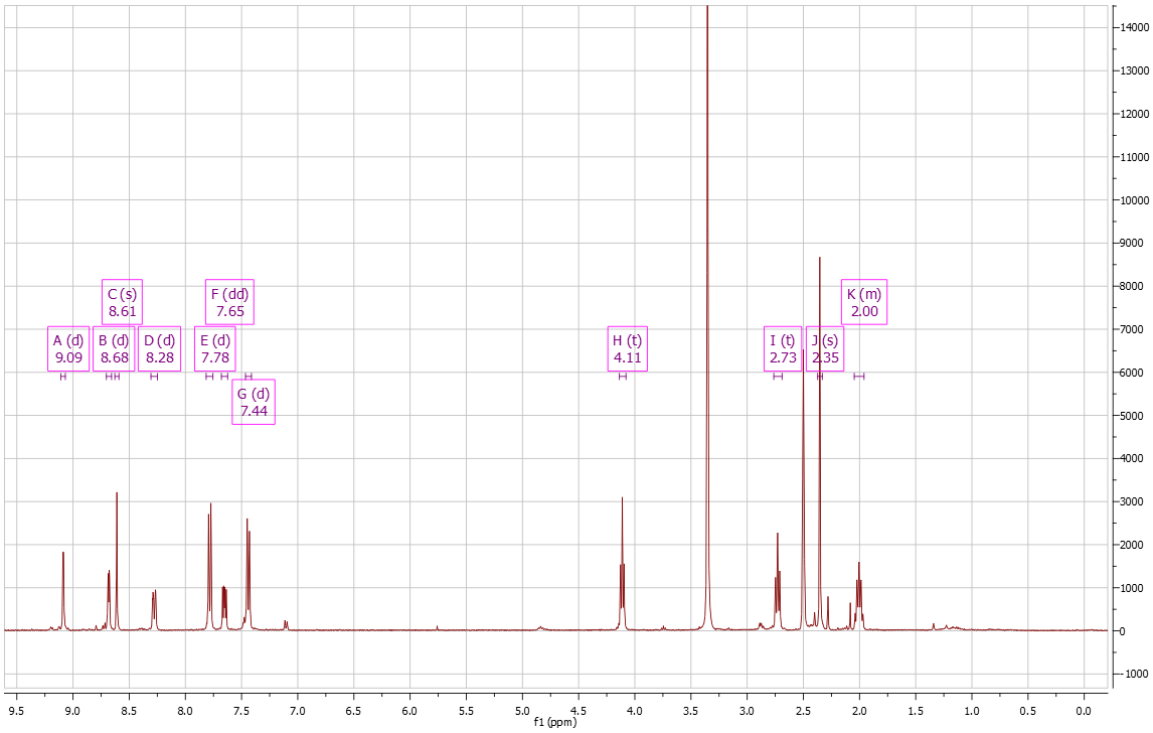

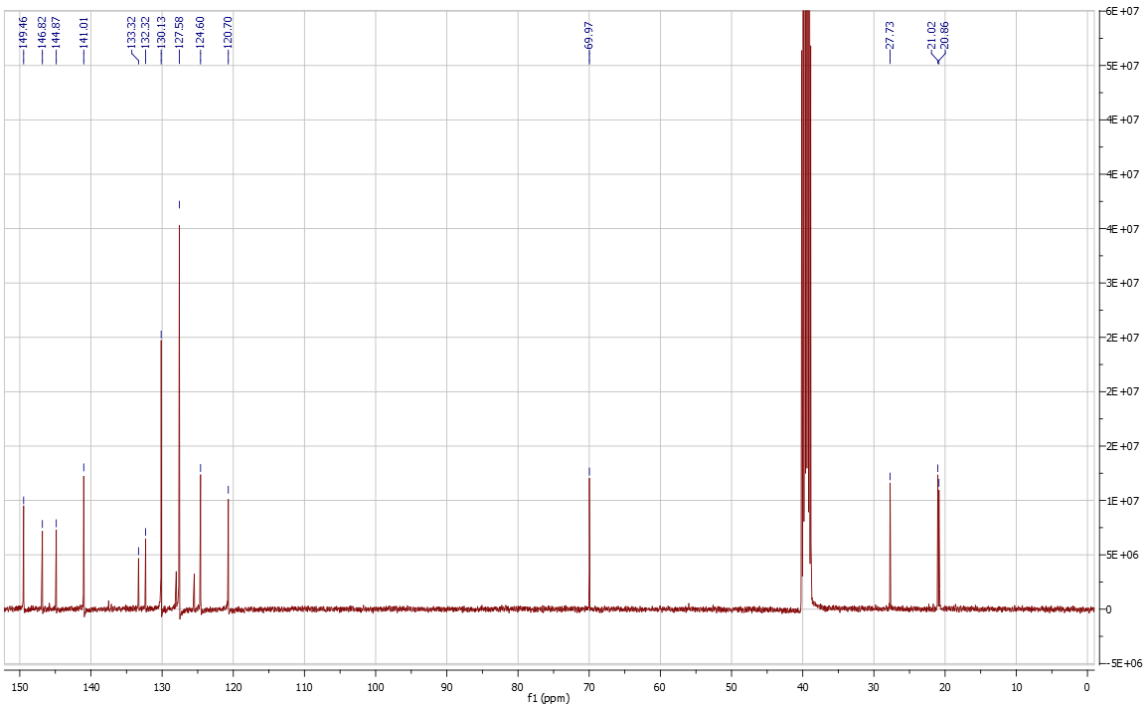


(53 mg, 30%). $^{1}$H NMR (400 MHz, DMSO-$d_6$) δ= 9.09 (d, *J* = 2.4 Hz, 1H), 8.68 (d, *J* = 3.5 Hz, 1H), 8.61 (s, 1H), 8.28 (d, *J* = 8.3 Hz, 1H), 7.78 (d, *J* = 8.2 Hz, 2H), 7.65 (dd, *J* = 8.3, 4.8 Hz, 1H), 7.44 (d, *J* = 8.1 Hz, 2H), 4.11 (t, *J* = 6.2 Hz, 2H), 2.73 (t, *J* = 7.5 Hz, 2H), 2.35 (s, 3H), 2.05 – 1.96 (m, 2H). $^{13}$C NMR (100 MHz, DMSO-$d_6$) δ= 149.46, 146.82, 144.87, 141.01, 133.32, 132.32, 130.13, 127.58, 124.60, 120.70, 69.97, 27.73, 21.02, 20.86. $t_R$=1.1 min, 96%.

### 7.2.4: 2-(4-(3-(tosyloxy) propyl)-1H-1,2,3-triazol-1-yl)pyridine (19)

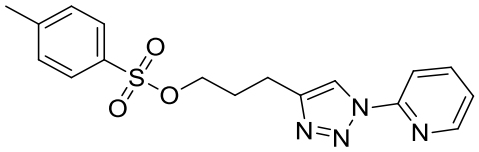

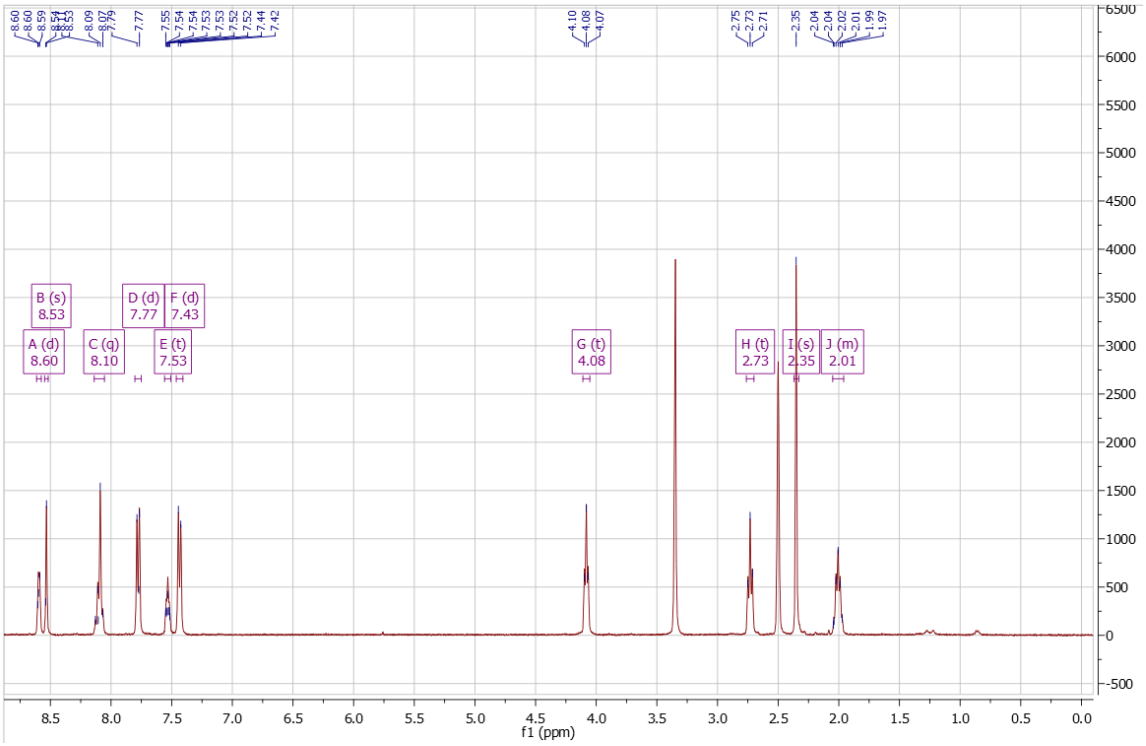

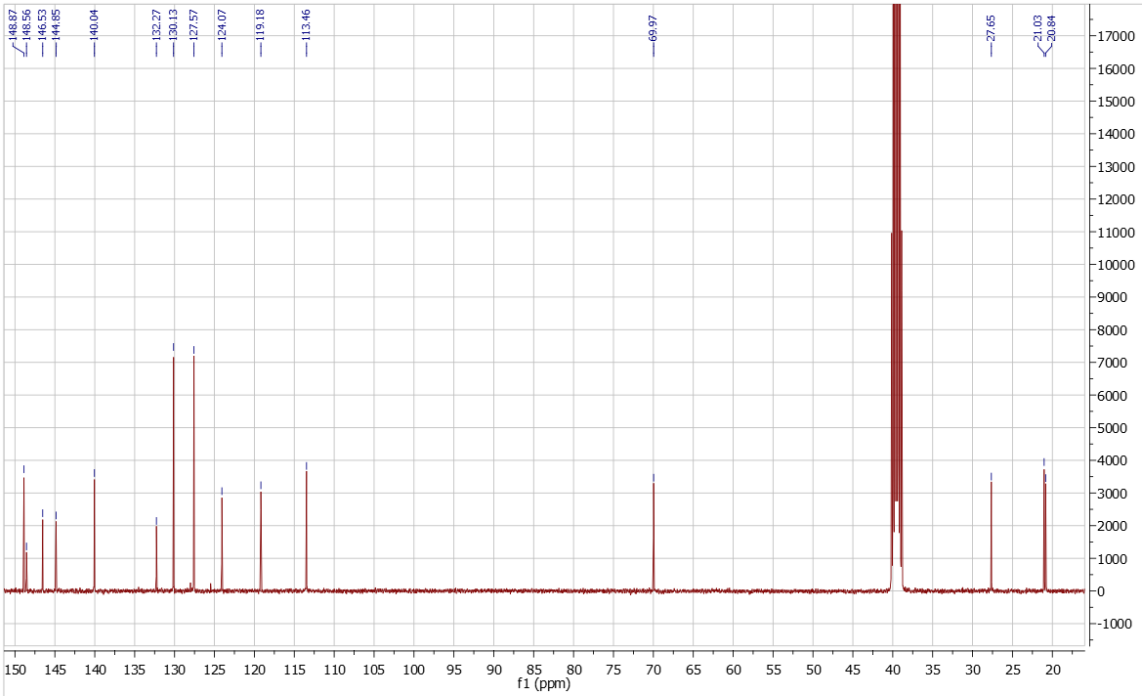


(47 mg, 27%). $^{1}$H NMR (400 MHz, DMSO-$d_6$) δ= 8.60 (d, *J* = 4.0 Hz, 1H), 8.53 (s, 1H), 8.10 (q, *J* = 16.1, 8.5 Hz, 2H), 7.77 (d, *J* = 7.9 Hz, 2H), 7.53 (t, *J* = 5.5 Hz, 1H), 7.43 (d, *J* = 8.0 Hz, 2H), 4.08 (t, *J* = 6.3 Hz, 2H), 2.73 (t, *J* = 7.6 Hz, 2H), 2.35 (s, 3H), 2.05 – 1.96 (m, 2H). $^{13}$C NMR (100 MHz, DMSO-$d_6$) δ= 148.87, 148.56, 146.53, 144.85, 140.04, 132.27, 130.13, 127.57, 124.07, 119.18, 113.46, 69.97, 27.65, 21.03, 20.84. $t_R$=0.36 min, 99%.

### 7.2.5: 2-(4-(3-(tosyloxy) propyl)-1H-1,2,3-triazol-1-yl)thiazole (20)

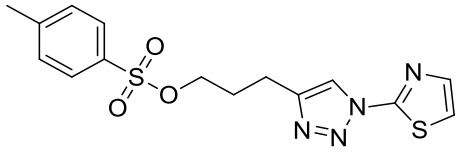

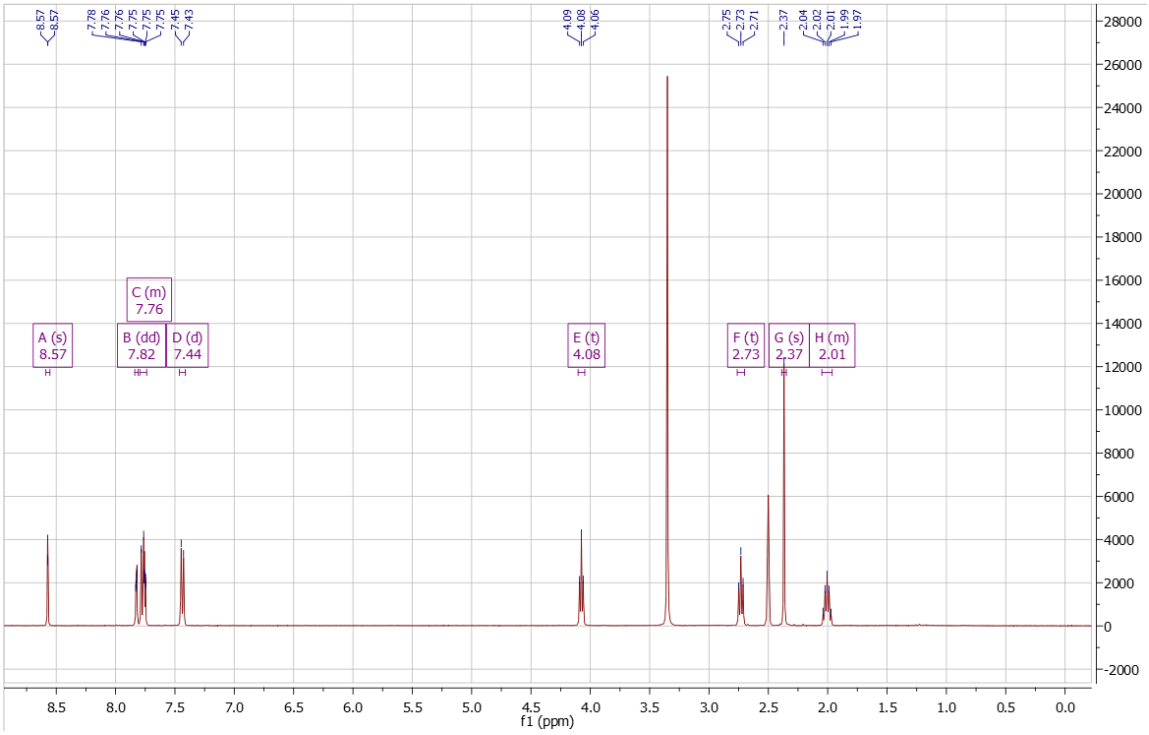

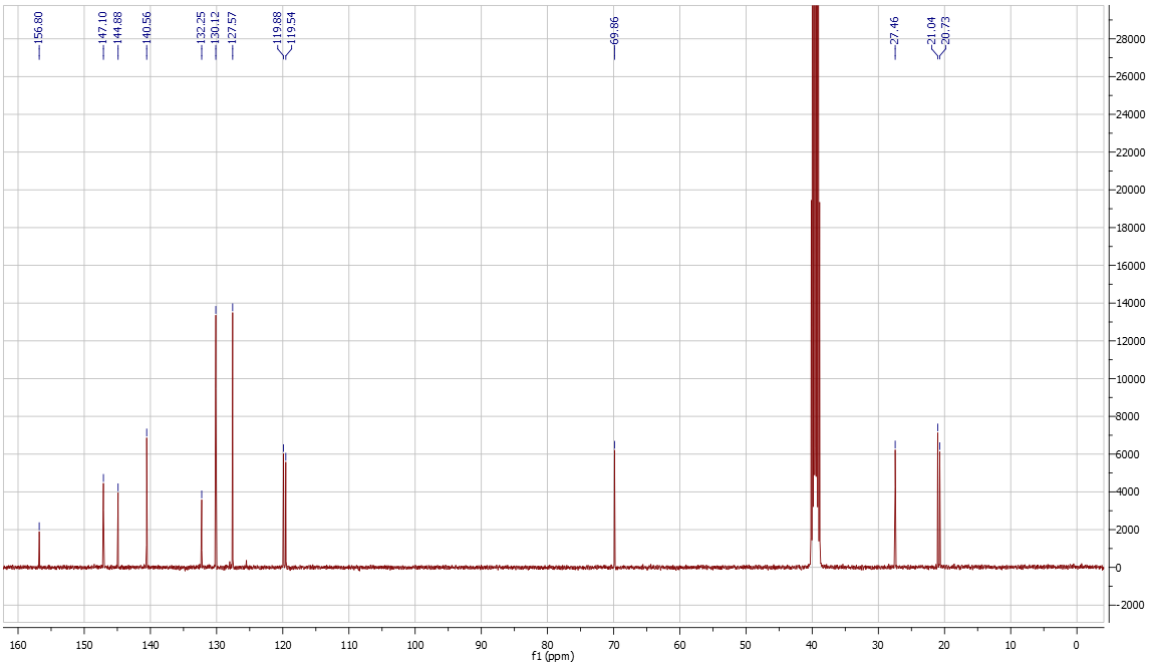


(69 mg, 57%). $^{1}$H NMR (400 MHz, DMSO-$d_6$) δ= 8.57 (s, 1H), 7.82 (dd, *J* = 3.5, 0.9 Hz, 1H), 7.80 – 7.74 (m, 3H), 7.44 (d, *J* = 8.0 Hz, 2H), 4.08 (t, *J* = 6.2 Hz, 2H), 2.73 (t, *J* = 7.5 Hz, 2H), 2.37 (s, 3H), 2.05 – 1.96 (m, 2H). $^{13}$C NMR (100 MHz, DMSO-$d_6$) δ= 156.80, 147.10, 144.88, 140.56, 132.25, 130.12, 127.57, 119.88, 119.54, 69.86, 27.46, 21.04, 20.73. $t_R$=0.35 min, 99%.

## 7.3: 1H and C13 NMR for Amides (23-30)

### 7.3.1: Methyl 4-(4-(3-(*N*-3-pyridinylamido)propyl)-1H-1,2,3-triazol-1-yl)benzoate (23)

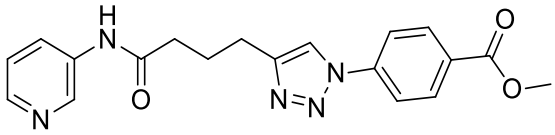

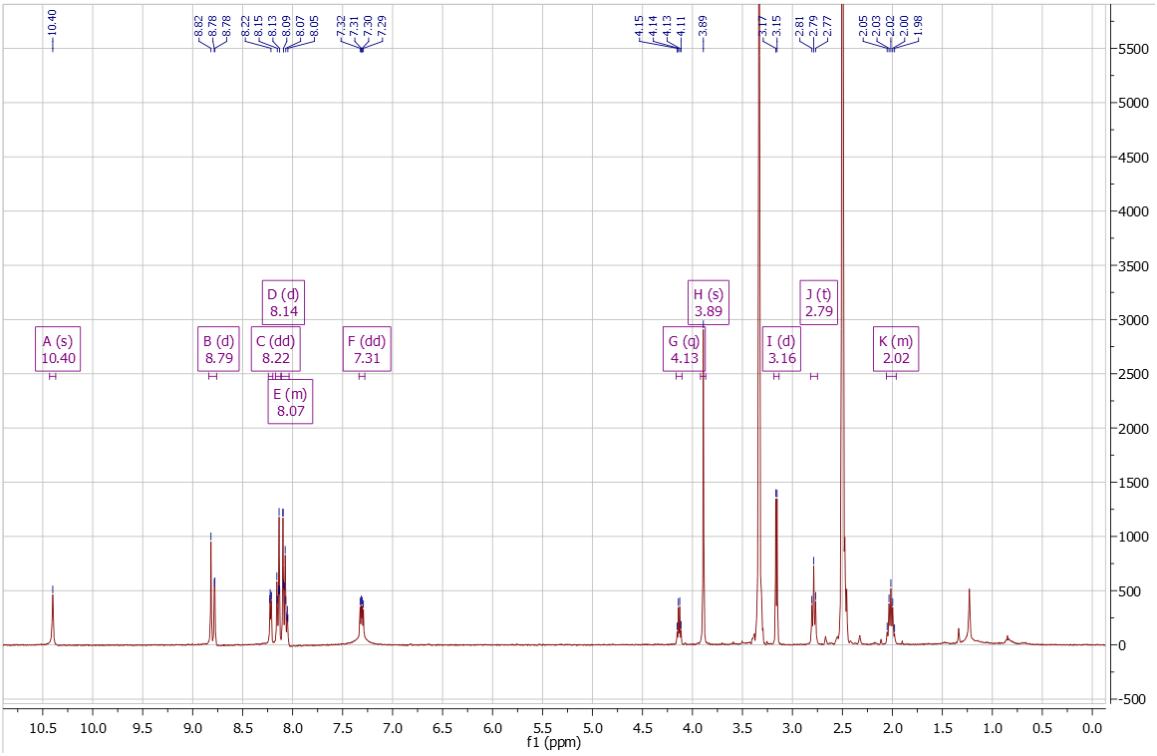

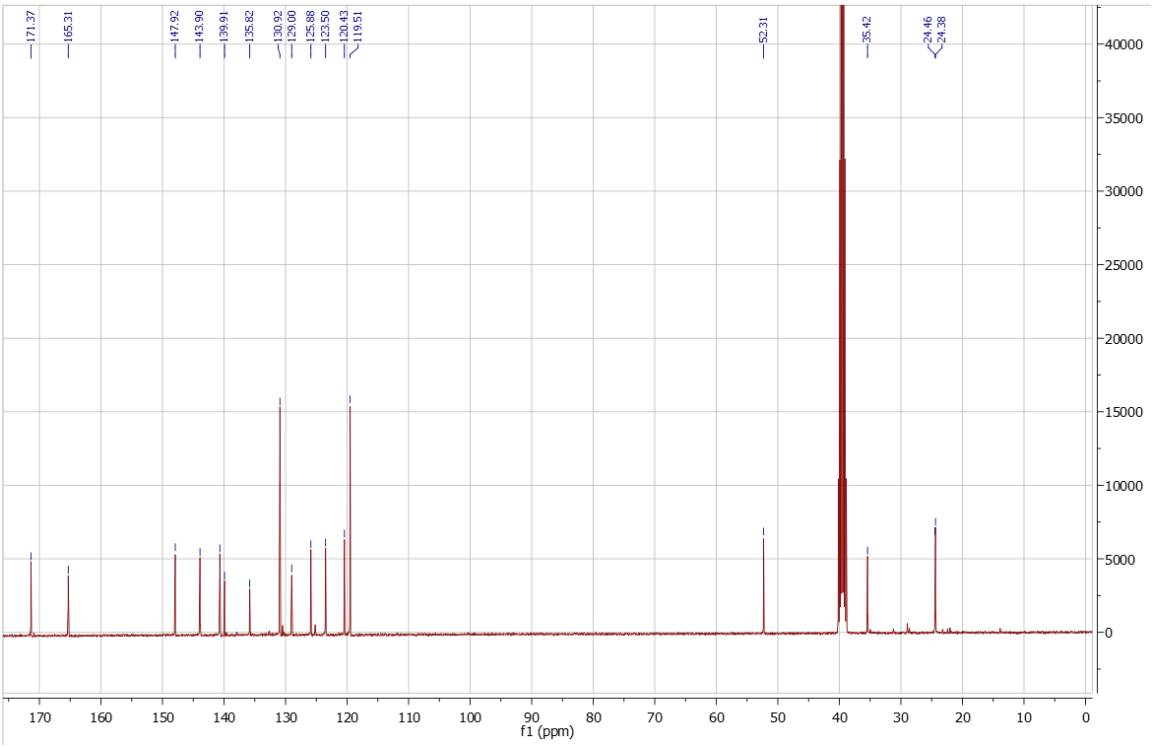


(28.9 mg, 46%). $^{1}$H NMR (400 MHz, DMSO-$d_6$) δ= 11.04 (s, 1H), 8.85 (s, 1H), 8.42 (d, *J* = 6.3 Hz, 2H), 8.12 (q, *J* = 17.7, 8.8 Hz, 4H), 7.72 (d, *J* = 6.5 Hz, 2H), 3.88 (s, 3H), 3.15 (s, 1H), 2.78 (t, *J* = 7.4 Hz, 2H), 2.54 (t, *J* = 7.5 Hz, 2H), 2.06 – 1.96 (m, 2H). $^{13}$C NMR (100 MHz, DMSO-$d_6$) δ= 171.37, 165.31, 147.92, 143.90, 140.68, 139.91, 135.82, 130.92, 129.00, 125.88, 123.50, 120.43, 119.51, 52.31, 35.42, 24.46, 24.38. $t_R$=3.8 min, 96%.

### 7.3.2: Methyl 4-(4-(3-(*N*-4-pyridinylamido)propyl)-1H-1,2,3-triazol-1-yl)benzoate (24)

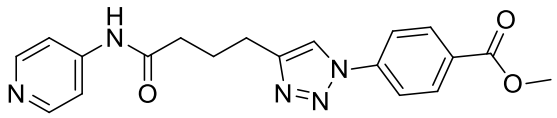

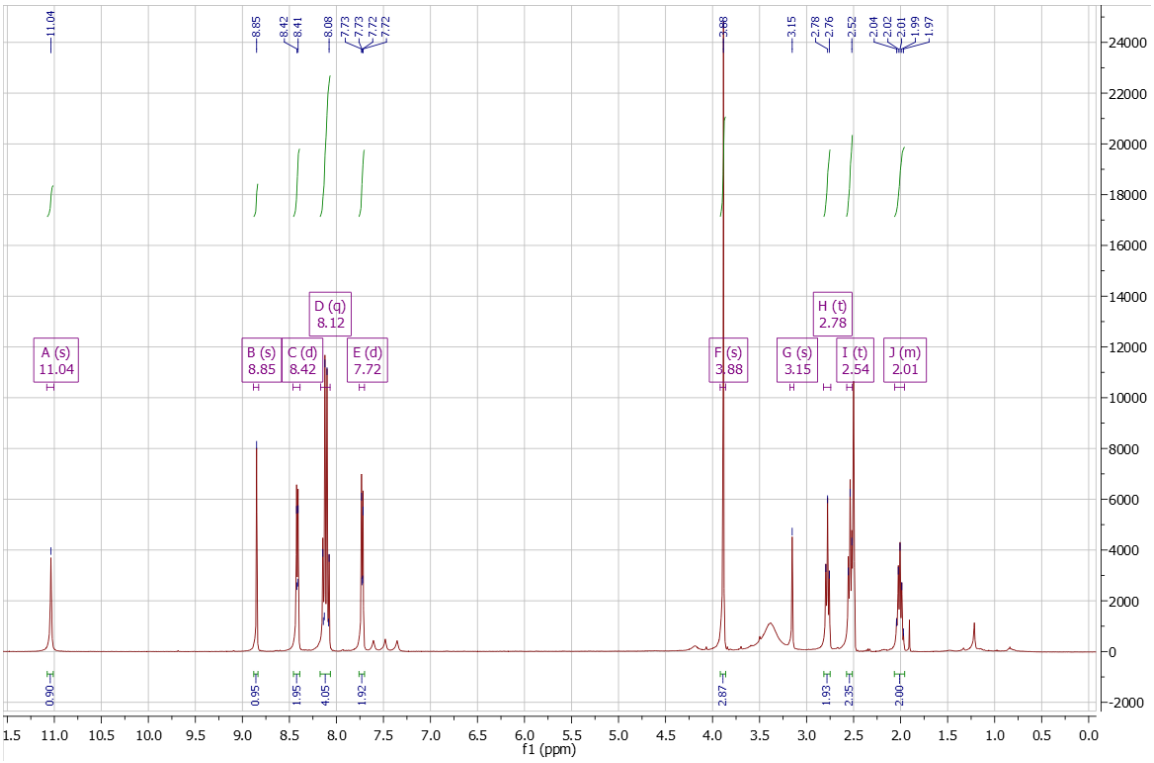

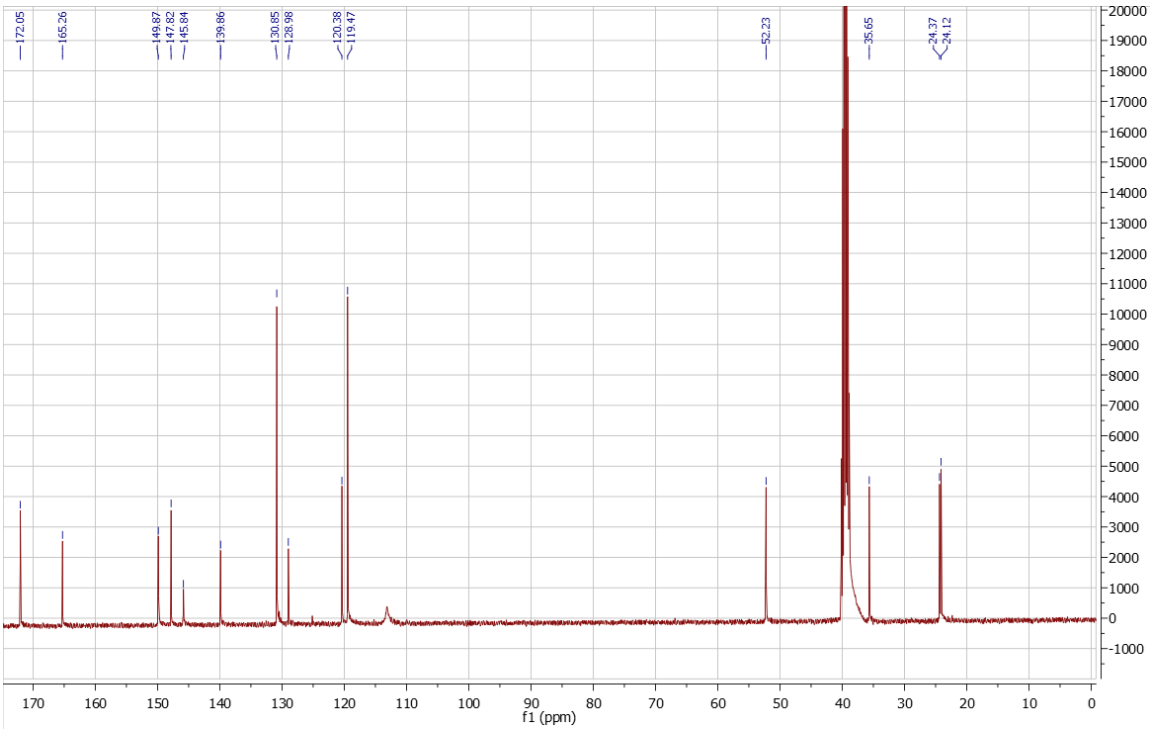


(23.9 mg, 38%). $^{1}$H NMR (400 MHz, DMSO-$d_6$) δ= 11.04 (s, 1H), 8.85 (s, 1H), 8.42 (d, *J* = 6.3 Hz, 2H), 8.12 (q, *J* = 17.7, 8.8 Hz, 4H), 7.72 (d, *J* = 6.5 Hz, 2H), 3.88 (s, 3H), 3.15 (s, 1H), 2.78 (t, *J* = 7.4 Hz, 2H), 2.54 (t, *J* = 7.5 Hz, 2H), 2.06 – 1.96 (m, 2H). $^{13}$C NMR (100 MHz, DMSO-$d_6$) δ= 172.05, 165.26, 149.87, 147.82, 145.84, 139.86, 130.85, 128.98, 120.38, 119.47, 52.23, 35.65, 24.37, 24.12. $t_R$=3.9 min, 97%.

### 7.3.3: Methyl 4-(4-(3-(*N*-4-pyridinylamido)propyl)-1H-1,2,3-triazol-1-yl)benzoate (25)

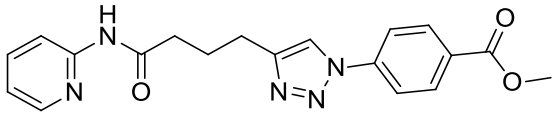

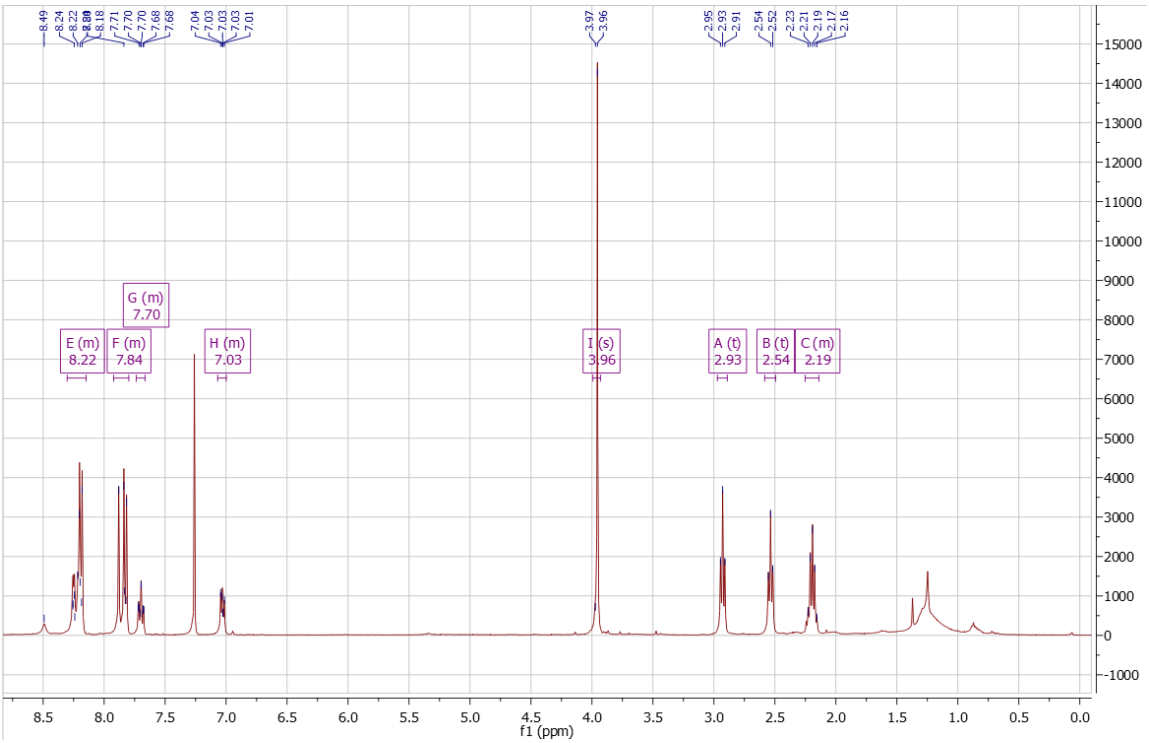

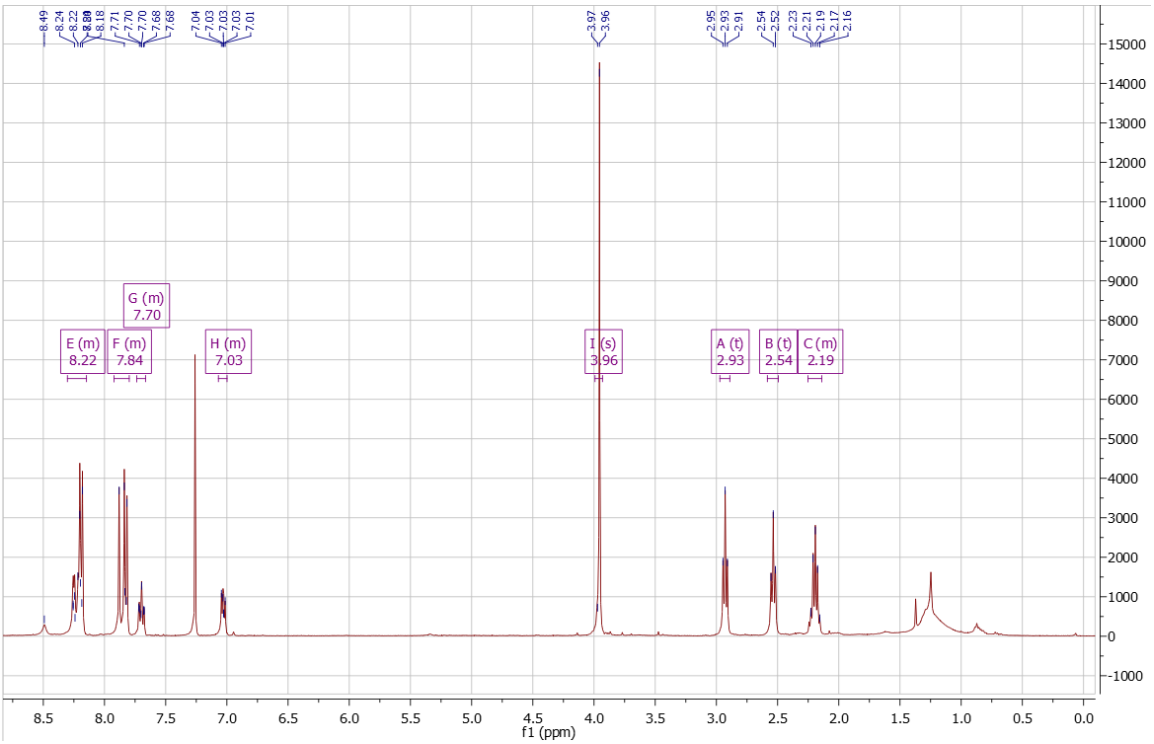


(39 mg, 31%). $^{1}$H NMR (400 MHz, $CDCl_3$) δ= 8.30 – 8.15 (m, 4H), 7.92 – 7.80 (m, 4H), 7.74 – 7.66 (m, 1H), 7.07 – 7.00 (m, 1H), 3.96 (s, 3H), 2.93 (t, *J* = 7.2 Hz, 2H), 2.54 (t, *J* = 7.2 Hz, 2H), 2.25 – 2.14 (m, 2H). $^{13}$C NMR (100 MHz, $CDCl_3$) δ= 171.99, 166.19, 155.22, 151.06, 148.33, 140.41, 131.54, 130.21, 119.97, 119.86, 119.47, 114.91, 52.64, 36.83, 24.98, 24.83, 18.66. $t_R$=5.0 min, 96%.

### 7.3.4: Methyl 4-(4-(3-(*N*-2-thiazolamido)propyl)-1H-1,2,3-triazol-1-yl)benzoate (26)

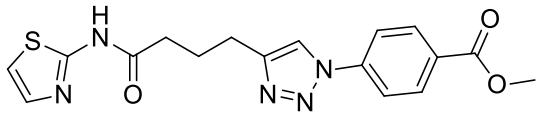

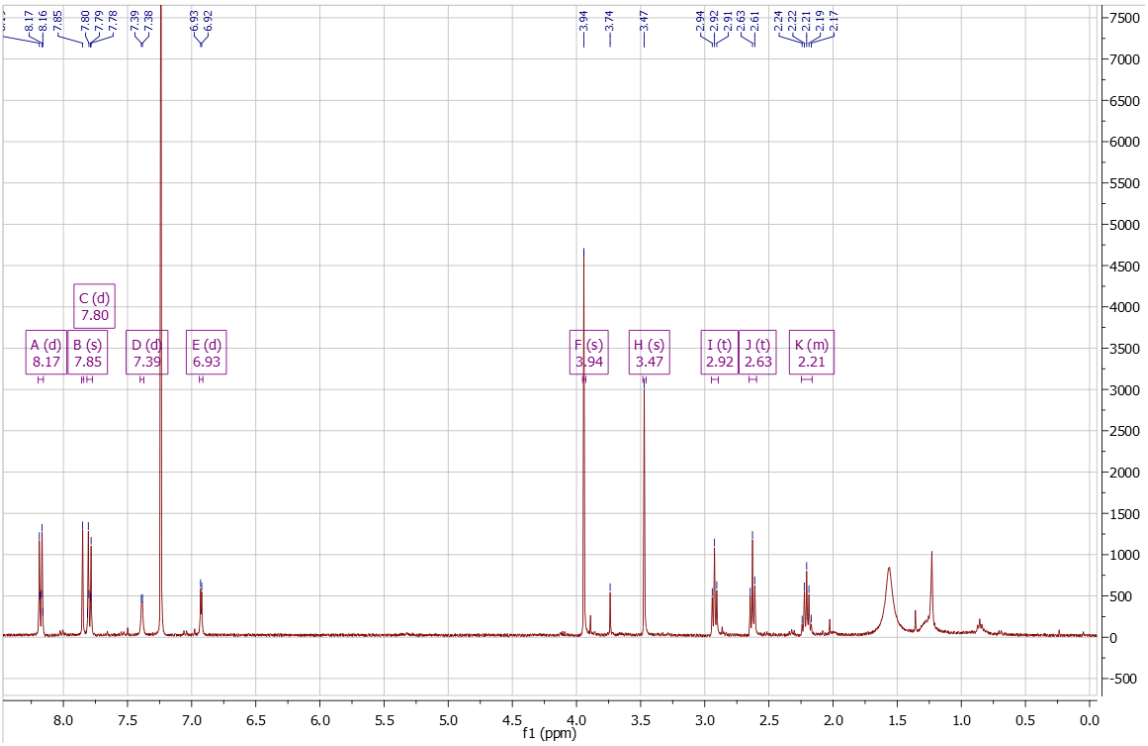


(66.5 mg, 52%). $^{1}$H NMR (400 MHz, $CDCl_3$) δ= 8.17 (d, *J* = 8.6 Hz, 2H), 7.85 (s, 1H), 7.80 (d, *J* = 8.6 Hz, 2H), 7.39 (d, *J* = 3.7 Hz, 1H), 6.93 (d, *J* = 3.6 Hz, 1H), 3.94 (s, 3H), 3.47 (s, 2H), 2.92 (t, *J* = 7.0 Hz, 2H), 2.63 (t, *J* = 7.1 Hz, 2H), 2.25 – 2.16 (m, 2H). $t_R$=2.3 min, 99%.

### 7.3.5: Methyl 4-(4-(3-(*N*-2-methoxypyridinylamido)propyl)-1H-1,2,3-triazol-1-yl)benzoate (27)

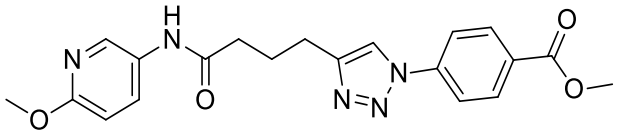

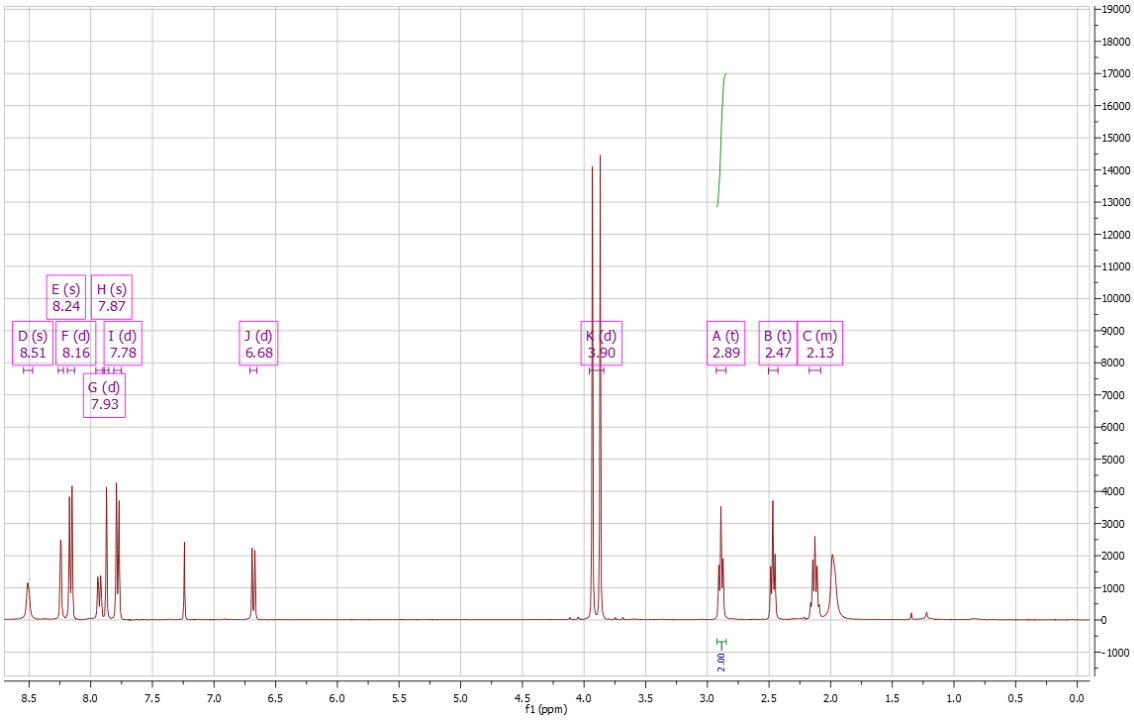

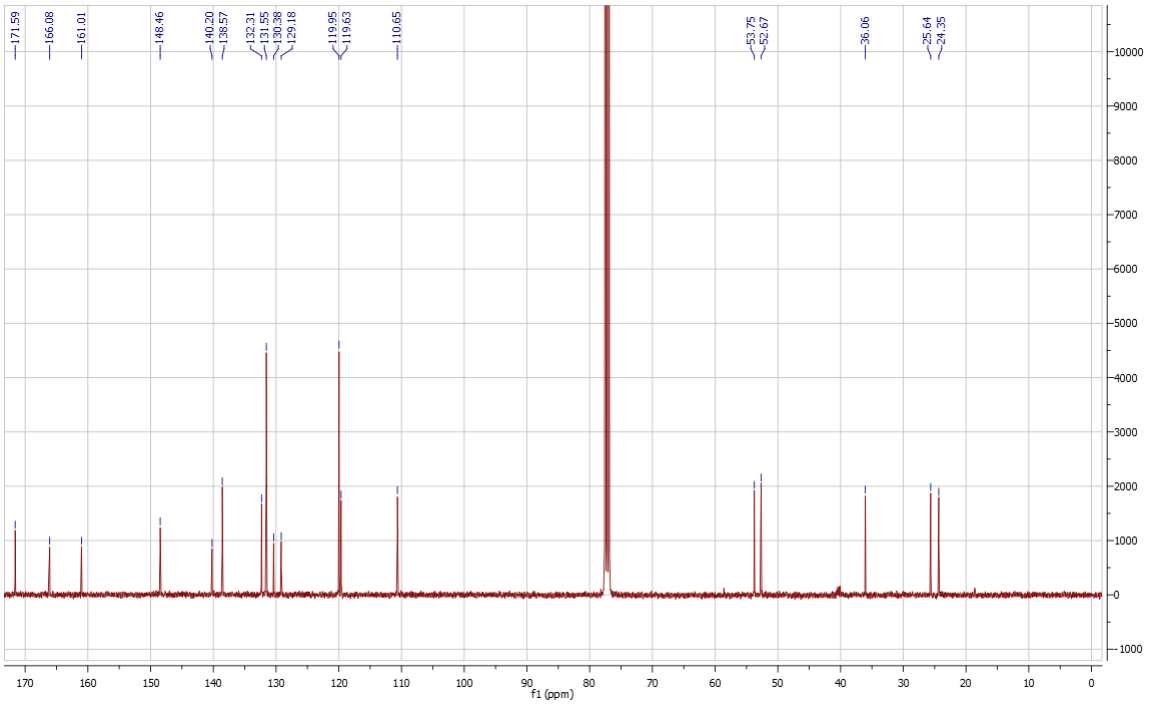


(32 mg, 23%).[1]H NMR (400 MHz, $CDCl_3$) δ= 8.51 (s, 1H, NH), 8.24 (s, 1H), 8.16 (d, *J* = 8.5 Hz, 2H), 7.93 (d, *J* = 8.9 Hz, 1H), 7.87 (s, 1H), 7.78 (d, *J* = 8.5 Hz, 2H), 6.68 (d, *J* = 8.9 Hz, 1H), 3.93 (s, 3H), 3.87 (s, 3H), 2.89 (t, *J* = 6.9 Hz, 2H), 2.47 (t, *J* = 7.0 Hz, 2H), 2.17 – 2.08 (m, 2H). [13]C NMR (100 MHz, $CDCl_3$) δ= 171.59, 166.08, 161.01, 148.46, 140.20, 138.57, 132.31, 131.55, 130.38, 129.18, 119.95, 119.63, 110.65, 53.75, 52.67, 36.06, 25.64, 24.35. $t_R$=4.8 min, 98%.

### 7.3.6: Methyl 4-(4-(3-(*N*-2-oxazolamido)propyl)-1H-1,2,3-triazol-1-yl)benzoate (28)

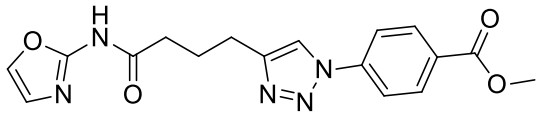

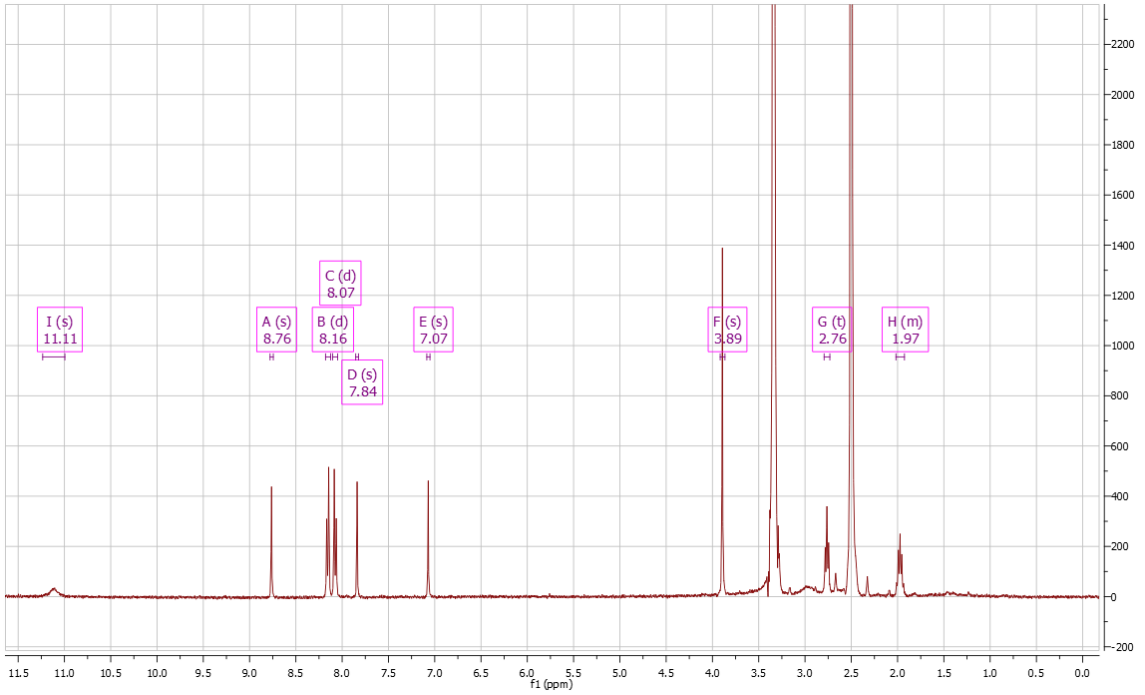


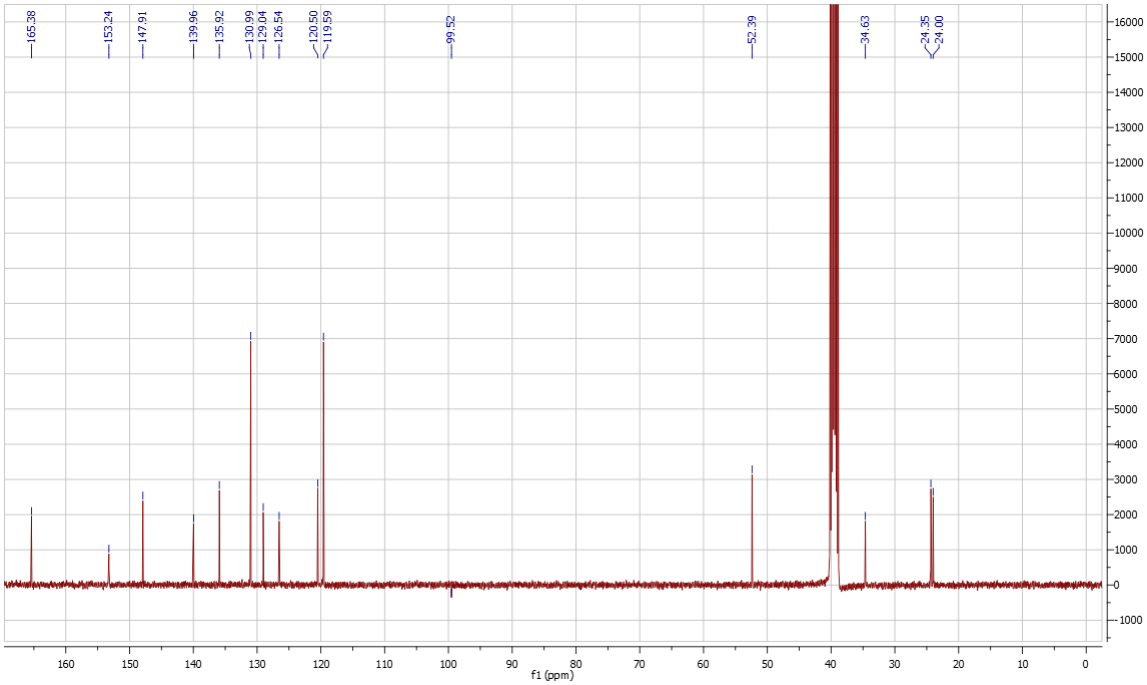

(20 mg, 16%). $^{1}$H NMR (400 MHz, DMSO-$d_6$) δ= 11.11 (s, 1H), 8.76 (s, 1H), 8.16 (d, *J* = 8.6 Hz, 2H), 8.07 (d, *J* = 8.6 Hz, 2H), 7.84 (s, 1H), 7.07 (s, 1H), 3.89 (s, 3H), 3.29 (t, 2H), 2.76 (t, *J* = 7.5 Hz, 2H), 2.02 – 1.93 (m, 2H). $^{13}$C NMR (100 MHz, DMSO-$d_6$) δ= 165.38, 153.24, 147.91, 139.96, 135.92, 130.99, 129.04, 126.54, 120.50, 119.59, 99.52, 52.39, 34.63, 24.35, 24.00. $t_R$=0.45 min, 99%

### 7.3.7: Methyl 4-(4-(3-(*N*-5-1,2,4-thiadiazolamido)propyl)-1H-1,2,3-triazol-1-yl)benzoate (29)

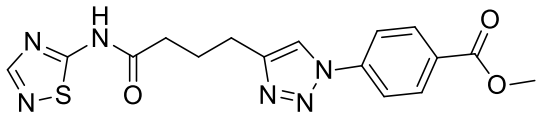

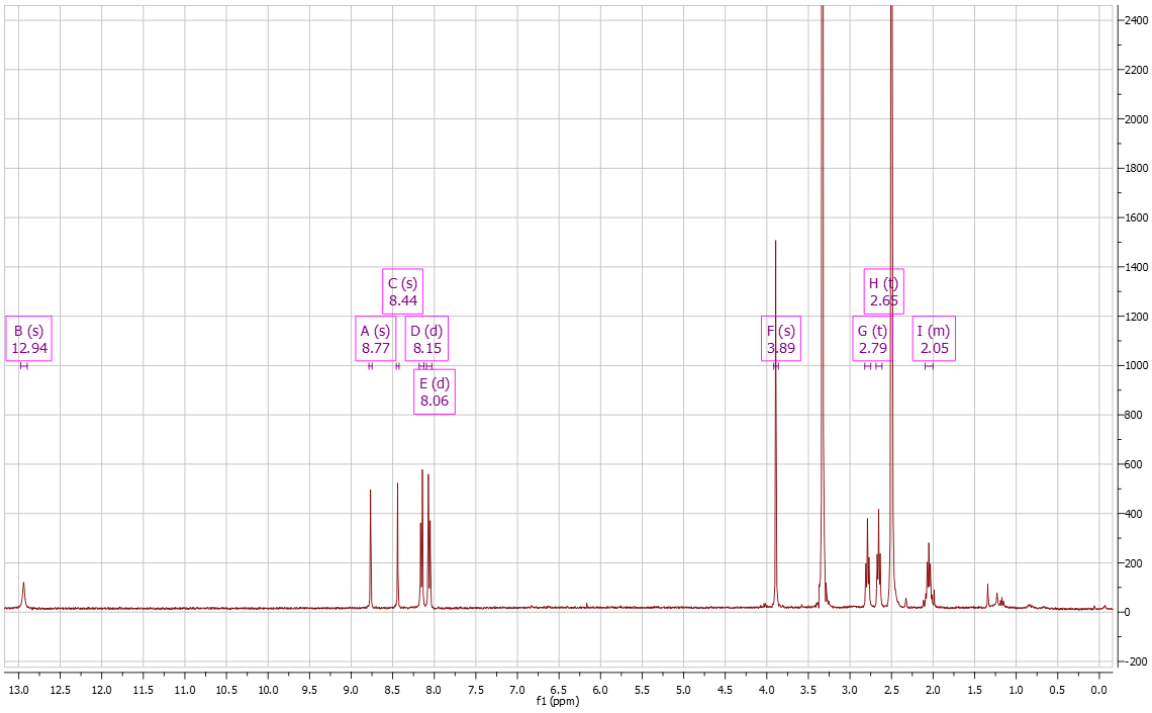

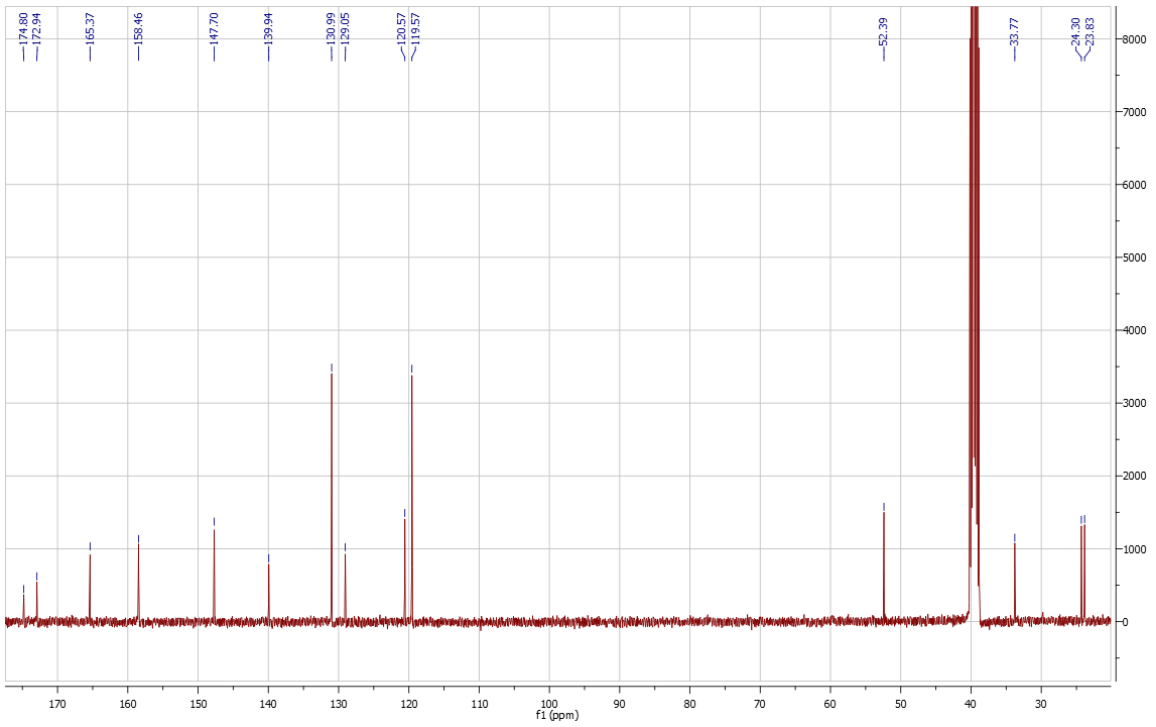


(29 mg, 23%). $^{1}$H NMR (400 MHz, DMSO-$d_6$) δ= 12.94 (s, 1H), 8.77 (s, 1H), 8.44 (s, 1H), 8.15 (d, *J* = 8.7 Hz, 2H), 8.06 (d, *J* = 8.8 Hz, 2H), 3.89 (s, 3H), 2.79 (t, *J* = 7.5 Hz, 2H), 2.65 (t, *J* = 7.3 Hz, 2H), 2.10 – 2.00 (m, 2H). $^{13}$C NMR (100 MHz, DMSO-$d_6$) δ= 174.80, 172.94, 165.37, 158.46, 147.70, 139.94, 130.99, 129.05, 120.57, 119.57, 52.39, 33.77, 24.30, 23.83. $t_R$=1.3 min, 99%.

### 7.3.8: Methyl 4-(4-(3-(*N*-4-pyrimidinylamido)propyl)-1H-1,2,3-triazol-1-yl)benzoate (30)

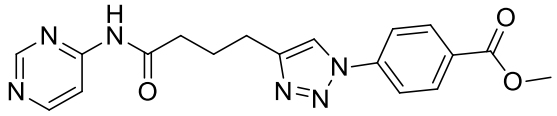

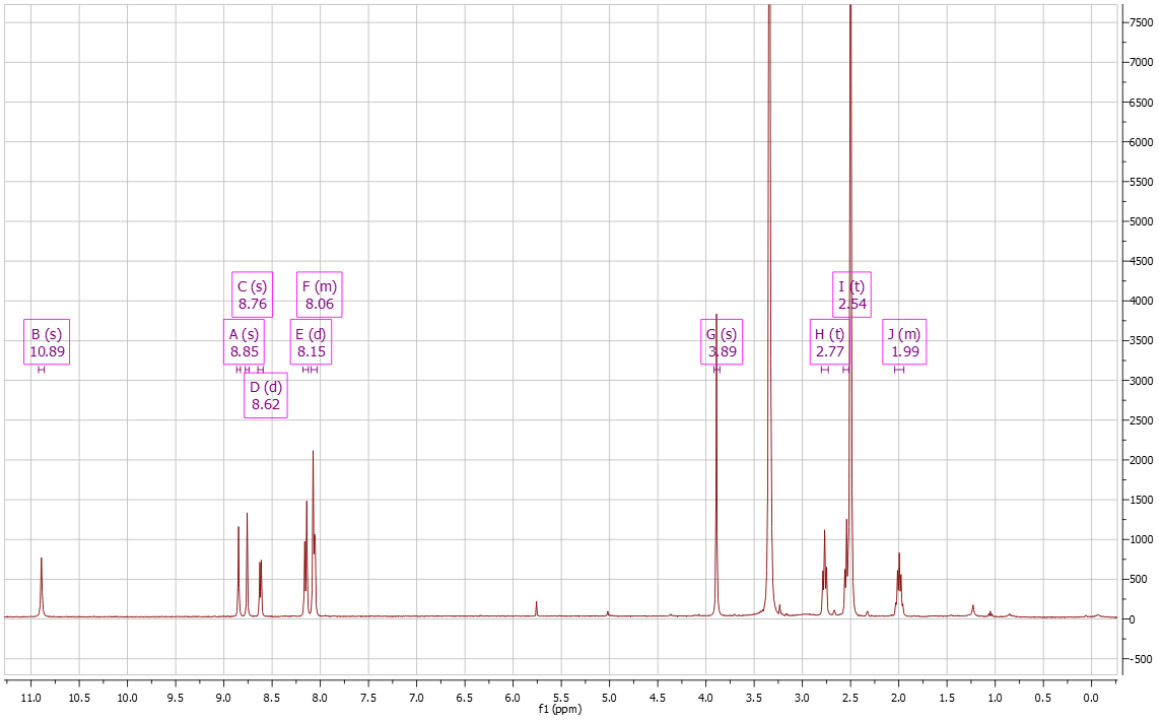

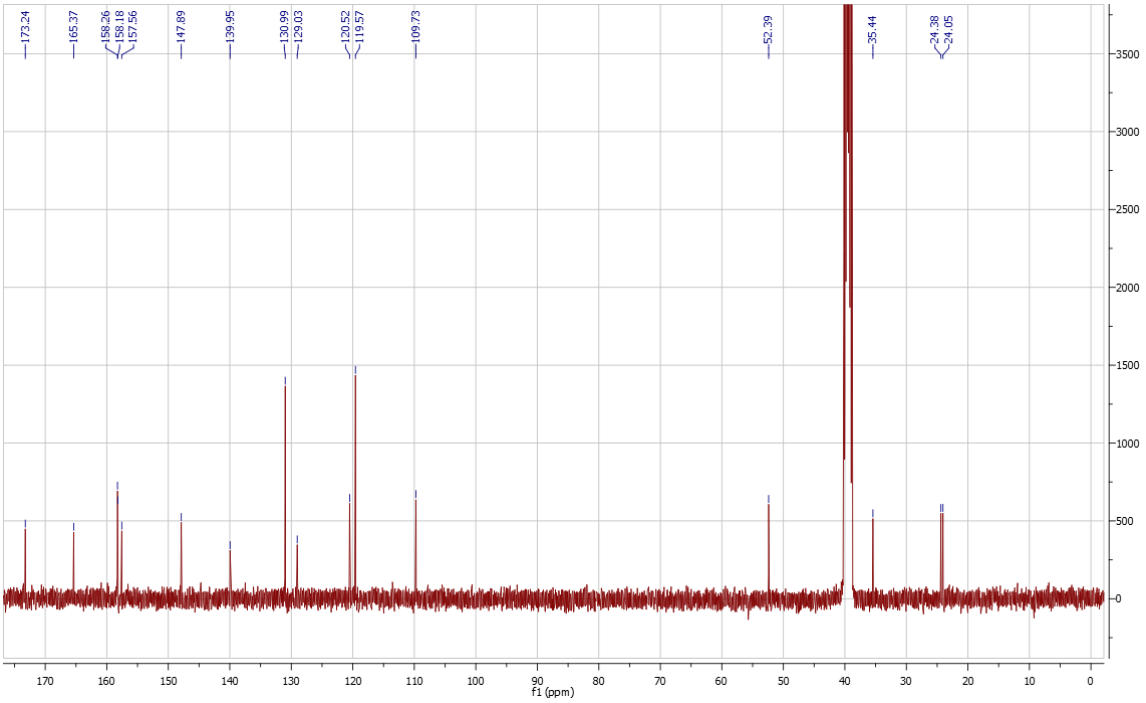


(14 mg, 11%). $^{1}$H NMR (400 MHz, DMSO-$d_6$) δ= 10.89 (s, 1H), 8.85 (s, 1H), 8.76 (s, 1H), 8.62 (d, *J* = 5.7 Hz, 1H), 8.15 (d, *J* = 8.3 Hz, 2H), 8.09 – 8.03 (m, 3H), 3.89 (s, 3H), 2.77 (t, *J* = 7.4 Hz, 2H), 2.54 (t, *J* = 7.3 Hz, 2H), 2.04 – 1.95 (m, 2H). $^{13}$C NMR (100 MHz, DMSO-$d_6$) δ= 173.24, 165.37, 158.26, 158.18, 157.56, 147.89, 139.95, 130.99, 129.03, 120.52, 119.57, 109.73, 52.39, 35.44, 24.38, 24.05. $t_R$=0.46 min, 99%

## References


(1) Braun, P.; Gingras, A.-C. History of Protein-Protein Interactions: From Egg-White to Complex Networks. *Proteomics* **2012**, *12* (10), 1478–1498.

(2) Garner, A. L.; Janda, K. D. Protein-Protein Interactions and Cancer: Targeting the Central Dogma. *Curr. Top. Med. Chem.* **2011**, *11* (3), 258–280.

(3) What Is Cancer? - National Cancer Institute https://www.cancer.gov/about-cancer/understanding/what-is-cancer (accessed Jun 28, 2020).

(4) Ivanov, A. A.; Khuri, F. R.; Fu, H. Targeting Protein-Protein Interactions as an Anticancer Strategy. *Trends Pharmacol. Sci.* **2013**, *34* (7), 393–400.

(5) Kline, M. P.; Rajkumar, S. V.; Timm, M. M.; Kimlinger, T. K.; Haug, J. L.; Lust, J. A.; Greipp, P. R.; Kumar, S. ABT-737, an Inhibitor of Bcl-2 Family Proteins, Is a Potent Inducer of Apoptosis in Multiple Myeloma Cells. *Leukemia* **2007**, *21* (7), 1549–1560.

(6) Tse, C.; Shoemaker, A. R.; Adickes, J.; Anderson, M. G.; Chen, J.; Jin, S.; Johnson, E. F.; Marsh, K. C.; Mitten, M. J.; Nimmer, P.; Roberts, L.; Tahir, S. K.; Xiao, Y.; Yang, X.; Zhang, H.; Fesik, S.; Rosenberg, S. H.; Elmore, S. W. ABT-263: A Potent and Orally Bioavailable Bcl-2 Family Inhibitor. *Cancer Res.* **2008**, *68* (9), 3421–3428.

(7) Souers, A. J.; Leverson, J. D.; Boghaert, E. R.; Ackler, S. L.; Catron, N. D.; Chen, J.; Dayton, B. D.; Ding, H.; Enschede, S. H.; Fairbrother, W. J.; Huang, D. C. S.; Hymowitz, S. G.; Jin, S.; Khaw, S. L.; Kovar, P. J.; Lam, L. T.; Lee, J.; Maecker, H. L.; Marsh, K. C.; Mason, K. D.; Mitten, M. J.; Nimmer, P. M.; Oleksijew, A.; Park, C. H.; Park, C.-M.; Phillips, D. C.; Roberts, A. W.; Sampath, D.; Seymour, J. F.; Smith, M. L.; Sullivan, G. M.; Tahir, S. K.; Tse, C.; Wendt, M. D.; Xiao, Y.; Xue, J. C.; Zhang, H.; Humerickhouse, R. A.; Rosenberg, S. H.; Elmore, S. W. ABT-199, a Potent and Selective BCL-2 Inhibitor, Achieves Antitumor Activity While Sparing Platelets. *Nat. Med.* **2013**, *19* (2), 202–208.

(8) Ho, S. W.; Tsui, Y. T. C.; Wong, T. T.; Cheung, S. K.-K.; Goggins, W. B.; Yi, L. M.; Cheng, K. K.; Baum, L. Effects of 17-Allylamino-17-Demethoxygeldanamycin (17-AAG) in Transgenic Mouse Models of Frontotemporal Lobar Degeneration and Alzheimer's Disease. *Transl. Neurodegener.* **2013**, *2*, 24.

(9) Secchiero, P.; di Iasio, M. G.; Gonelli, A.; Zauli, G. The MDM2 Inhibitor Nutlins as an Innovative Therapeutic Tool for the Treatment of Haematological Malignancies. *Curr. Pharm. Des.* **2008**, *14* (21), 2100–2110.

(10) Lozano, G.; Zambetti, G. P. Gankyrin: An Intriguing Name for a Novel Regulator of P53 and RB. *Cancer Cell* **2005**, *8* (1), 3–4.

(11) Higashitsuji, H.; Itoh, K.; Nagao, T.; Dawson, S.; Nonoguchi, K.; Kido, T.; Mayer, R. J.; Arii, S.; Fujita, J. Reduced Stability of Retinoblastoma Protein by Gankyrin,

an Oncogenic Ankyrin-Repeat Protein Overexpressed in Hepatomas. *Nat. Med.* **2000**, *6* (1), 96–99.
(12) Dawson, S.; Higashitsuji, H.; Wilkinson, A. J.; Fujita, J.; Mayer, R. J. Gankyrin: A New Oncoprotein and Regulator of PRb and P53. *Trends Cell Biol.* **2006**, *16* (5), 229–233.
(13) Liu, Y.; Zhang, J.; Qian, W.; Dong, Y.; Yang, Y.; Liu, Z.; Feng, Y.; Ma, D.; Zhang, Z.; Wu, S. Gankyrin Is Frequently Overexpressed in Cervical High Grade Disease and Is Associated with Cervical Carcinogenesis and Metastasis. *PLOS ONE* **2014**, *9* (4), e95043.
(14) Kim, Y. H.; Kim, J.-H.; Choi, Y. W.; Lim, S. K.; Yim, H.; Kang, S. Y.; Chung, Y. S.; Lee, G.-Y.; Park, T. J. Gankyrin Is Frequently Overexpressed in Breast Cancer and Is Associated with ErbB2 Expression. *Exp. Mol. Pathol.* **2013**, *94* (2), 360–365.
(15) Ortiz, C. M.; Tsunoda, S.; Tanaka, E.; Ito, T.; Higashitsuji, H.; Fujita, J.; Shimada, Y.; Sakai, Y. Overexpression of the Novel Oncoprotein Gankyrin in Human Esophageal Squamous Cell Carcinoma (ESCC) and Its Clinical Significance. *Cancer Res.* **2006**, *66* (8 Supplement), 997–998.
(16) Huang, B.; Cai, W.; Wang, Q.; Liu, F.; Xu, M.; Zhang, Y. Gankyrin Drives Malignant Transformation of Gastric Cancer and Alleviates Oxidative Stress via mTORC1 Activation https://www.hindawi.com/journals/omcl/2018/9480316/ (accessed May 7, 2020).
(17) Livneh, I.; Cohen-Kaplan, V.; Cohen-Rosenzweig, C.; Avni, N.; Ciechanover, A. The Life Cycle of the 26S Proteasome: From Birth, through Regulation and Function, and onto Its Death. *Cell Res.* **2016**, *26* (8), 869–885.
(18) Naujokat, C.; Hoffmann, S. Role and Function of the 26S Proteasome in Proliferation and Apoptosis. *Lab. Invest.* **2002**, *82* (8), 965–980.
(19) Dawson, S.; Apcher, S.; Mee, M.; Higashitsuji, H.; Baker, R.; Uhle, S.; Dubiel, W.; Fujita, J.; Mayer, R. J. Gankyrin Is an Ankyrin-Repeat Oncoprotein That Interacts with CDK4 Kinase and the S6 ATPase of the 26 S Proteasome. *J. Biol. Chem.* **2002**, *277* (13), 10893–10902.
(20) Giacinti, C.; Giordano, A. RB and Cell Cycle Progression. *Oncogene* **2006**, *25* (38), 5220–5227.
(21) Graf, F.; Koehler, L.; Kniess, T.; Wuest, F.; Mosch, B.; Pietzsch, J. Cell Cycle Regulating Kinase Cdk4 as a Potential Target for Tumor Cell Treatment and Tumor Imaging. *J. Oncol.* **2009**, *2009*.
(22) Nitta, R. T.; Smith, C. L.; Kennedy, B. K. Evidence That Proteasome-Dependent Degradation of the Retinoblastoma Protein in Cells Lacking A-Type Lamins Occurs Independently of Gankyrin and MDM2. *PLOS ONE* **2007**, *2* (9), e963.
(23) Rubin, S. M. Deciphering the Rb Phosphorylation Code. *Trends Biochem. Sci.* **2013**, *38* (1), 12–19.

(24) Li, J.; Knobloch, T. J.; Kresty, L. A.; Zhang, Z.; Lang, J. C.; Schuller, D. E.; Weghorst, C. M. Gankyrin, A Biomarker for Epithelial Carcinogenesis, Is Overexpressed in Human Oral Cancer. *Anticancer Res.* **2011**, *31* (9), 2683–2692.
(25) Aubrey, B. J.; Kelly, G. L.; Janic, A.; Herold, M. J.; Strasser, A. How Does P53 Induce Apoptosis and How Does This Relate to P53-Mediated Tumour Suppression? *Cell Death Differ.* **2018**, *25* (1), 104–113.
(26) Higashitsuji, H.; Higashitsuji, H.; Itoh, K.; Sakurai, T.; Nagao, T.; Sumitomo, Y.; Sumitomo, H.; Masuda, T.; Dawson, S.; Shimada, Y.; Mayer, R. J.; Fujita, J. The Oncoprotein Gankyrin Binds to MDM2/HDM2, Enhancing Ubiquitylation and Degradation of P53. *Cancer Cell* **2005**, *8* (1), 75–87.
(27) Love, I. M.; Shi, D.; Grossman, S. R. P53 Ubiquitination and Proteasomal Degradation. *Methods Mol. Biol. Clifton NJ* **2013**, *962*, 63–73.
(28) Fridman, J. S.; Lowe, S. W. Control of Apoptosis by P53. *Oncogene* **2003**, *22* (56), 9030–9040.
(29) Higashitsuji, H.; Higashitsuji, H.; Liu, Y.; Masuda, T.; Fujita, T.; Abdel-Aziz, H. I.; Kongkham, S.; Dawson, S.; John Mayer, R.; Itoh, Y.; Sakurai, T.; Itoh, K.; Fujita, J. The Oncoprotein Gankyrin Interacts with RelA and Suppresses NF-KappaB Activity. *Biochem. Biophys. Res. Commun.* **2007**, *363* (3), 879–884.
(30) Yin, L.; Ma, H.; Ge, X.; Edwards, P. A.; Zhang, Y. Hepatic Hepatocyte Nuclear Factor 4α Is Essential for Maintaining Triglyceride and Cholesterol Homeostasis. *Arterioscler. Thromb. Vasc. Biol.* **2011**, *31* (2), 328–336.
(31) Yang, C.; Tan, Y.-X.; Yang, G.-Z.; Zhang, J.; Pan, Y.-F.; Liu, C.; Fu, J.; Chen, Y.; Ding, Z.-W.; Dong, L.-W.; Wang, H.-Y. Gankyrin Has an Antioxidative Role through the Feedback Regulation of Nrf2 in Hepatocellular Carcinoma. *J. Exp. Med.* **2016**, *213* (5), 859–875.
(32) Yagishita, Y.; Uruno, A.; Yamamoto, M. Chapter 27 - NRF2-Mediated Gene Regulation and Glucose Homeostasis. In *Molecular Nutrition and Diabetes*; Mauricio, D., Ed.; Academic Press: San Diego, 2016; pp 331–348.
(33) Zamani, P.; Matbou Riahi, M.; Momtazi-Borojeni, A. A.; Jamialahmadi, K. Gankyrin: A Novel Promising Therapeutic Target for Hepatocellular Carcinoma. *Artif. Cells Nanomedicine Biotechnol.* **2018**, *46* (7), 1301–1313.
(34) Li, H.; Zhang, J.; Zhen, C.; Yang, B.; Feng, L. Gankyrin as a Potential Target for Tumor Therapy: Evidence and Perspectives. *Am. J. Transl. Res.* **2018**, *10* (7), 1949–1960.
(35) Zeng, Y.-C.; Sun, D.; Li, W.-H.; Zhao, J.; Xin, Y. Gankyrin Promotes the Proliferation of Gastric Cancer and Is Associated with Chemosensitivity. *Tumour Biol. J. Int. Soc. Oncodevelopmental Biol. Med.* **2017**, *39* (6), 1010428317704820.
(36) Zheng, T.; Hong, X.; Wang, J.; Pei, T.; Liang, Y.; Yin, D.; Song, R.; Song, X.; Lu, Z.; Qi, S.; Liu, J.; Sun, B.; Xie, C.; Pan, S.; Li, Y.; Luo, X.; Li, S.; Fang, X.; Bhatta, N.; Jiang, H.; Liu, L. Gankyrin Promotes Tumor Growth and Metastasis through

Activation of IL-6/STAT3 Signaling in Human Cholangiocarcinoma. *Hepatology* **2014**, *59* (3), 935–946.
(37) Chapman, A. M.; McNaughton, B. R. Synthetic Proteins Potently and Selectively Bind the Oncoprotein Gankyrin, Modulate Its Interaction with S6 ATPase, and Suppress Gankyrin/MDM2-Dependent Ubiquitination of P53. *ACS Chem. Biol.* **2015**, *10* (8), 1880–1886.
(38) Wójcik, P.; Berlicki, Ł. Peptide-Based Inhibitors of Protein-Protein Interactions. *Bioorg. Med. Chem. Lett.* **2016**, *26* (3), 707–713.
(39) Chattopadhyay, A.; O'Connor, C. J.; Zhang, F.; Galvagnion, C.; Galloway, W. R. J. D.; Tan, Y. S.; Stokes, J. E.; Rahman, T.; Verma, C.; Spring, D. R.; Itzhaki, L. S. Discovery of a Small-Molecule Binder of the Oncoprotein Gankyrin That Modulates Gankyrin Activity in the Cell. *Sci. Rep.* **2016**, *6* (1), 23732.
(40) D'Souza, A. M.; Jiang, Y.; Cast, A.; Valanejad, L.; Wright, M.; Lewis, K.; Kumbaji, M.; Shah, S.; Smithrud, D.; Karns, R.; Shin, S.; Timchenko, N. Gankyrin Promotes Tumor-Suppressor Protein Degradation to Drive Hepatocyte Proliferation. *Cell. Mol. Gastroenterol. Hepatol.* **2018**, *6* (3), 239–255.
(41) Ma, W.; Yang, L.; He, L. Overview of the Detection Methods for Equilibrium Dissociation Constant KD of Drug-Receptor Interaction. *J. Pharm. Anal.* **2018**, *8* (3), 147–152.
(42) KD value: a quantitative measurement of antibody affinity | Abcam https://www.abcam.com/primary-antibodies/kd-value-a-quantitive-measurement-of-antibody-affinity (accessed Aug 31, 2020).
(43) Velagapudi, S. P.; Costales, M. G.; Vummidi, B. R.; Nakai, Y.; Angelbello, A. J.; Tran, T.; Haniff, H. S.; Matsumoto, Y.; Wang, Z. F.; Chatterjee, A. K.; Childs-Disney, J. L.; Disney, M. D. Approved Anti-Cancer Drugs Target Oncogenic Non-Coding RNAs. *Cell Chem. Biol.* **2018**, *25* (9), 1086-1094.e7.
(44) 24.4: Hydrolysis of Amides https://chem.libretexts.org/Bookshelves/Organic_Chemistry/Book%3A_Basic_Principles_of_Organic_Chemistry_(Roberts_and_Caserio)/24%3A_Organonitrogen_Compounds_II-_Amides%2C_Nitriles%2C__Nitro_Compounds/24.04%3A_Hydrolysis_of_Amides (accessed Jun 9, 2020).
(45) Mahesh, S.; Tang, K.-C.; Raj, M. Amide Bond Activation of Biological Molecules. *Mol. J. Synth. Chem. Nat. Prod. Chem.* **2018**, *23* (10).
(46) Alcohol Reactivity https://www2.chemistry.msu.edu/faculty/reusch/VirtTxtJml/alcohol1.htm (accessed Jun 28, 2020).
(47) Jia, Z.; Zhu, Q. 'Click' Assembly of Selective Inhibitors for MAO-A. *Bioorg. Med. Chem. Lett.* **2010**, *20* (21), 6222–6225.

(48) Pyrtriazoles, a Novel Class of Store-Operated Calcium Entry Modulators: Discovery, Biological Profiling, and in Vivo Proof-of-Concept Efficacy in Acute Pancreatitis | Journal of Medicinal Chemistry https://pubs.acs.org/doi/abs/10.1021/acs.jmedchem.8b01512 (accessed Jun 24, 2020).
(49) BioByte ClogP http://www.biobyte.com/bb/prod/40manual.pdf (accessed Aug 24, 2020).
(50) Avdeef, A.; Box, K. J.; Comer, J. E.; Hibbert, C.; Tam, K. Y. PH-Metric LogP 10. Determination of Liposomal Membrane-Water Partition Coefficients of Ionizable Drugs. *Pharm. Res.* **1998**, *15* (2), 209–215.

**VITA**

| | |
|---|---|
| Name: | Daniel (Yi-Chih) Juang |
| Baccalaureate Degree: | Bachelor of Science, St. John's University, Jamaica, Major: Biology |
| Date Graduated: | January, 2016 |
| High School: | École active Bilingue – The Victor Hugo School (now École Internationale Bilingue – The Victor Hugo School), Paris, France |
| Date Graduated: | May 2010 |